Research Square

Preprints are preliminary reports that have not undergone peer review.
They should not be considered conclusive, used to inform clinical practice,
or referenced by the media as validated information.

Performance Analysis of Spatial Diversity-Based Free Space Optical Communications Systems for Various Atmospheric Turbulence Models with Pointing Errors

Moataz M. Roshdy

moatazroshdy2015@mtc.edu.eg

Military Technical College

Mohamed Ebead

Military Technical College

Mostafa Thabet

Military Technical College

Khaled A. Ghorib

Military Technical College

Ahmed Elshweikh

Military Technical College

Mohamed Shoueib

Military Technical College

Aly R. Elmetwaly

Military Technical College

Haitham Khallaf

Saxony Egypt University for Applied Science and Technology

Ahmed Elghandor

Military Technical College

Article

Keywords:

Posted Date: November 6th, 2026

DOI: https://doi.org/10.21203/rs.3.rs-11608904/v1

License: This work is licensed under a Creative Commons Attribution 4.0 International License.
Read Full License

Additional Declarations: No competing interests reported.

Performance Analysis of Spatial Diversity-Based Free Space Optical Communications Systems for Various Atmospheric Turbulence Models with Pointing Errors

Moataz M. Roshdy[1*], Mohamed Ebead[1], Mostafa Thabet[1], Khaled A. Ghorib[1], Ahmed Elshweikh[1], Mohamed Shoueib[1], Aly R. Elmetwaly[1], Haitham Khallaf[2], Ahmed Elghandor[1]

[1*]Department of Communications Engineering, Military Technical College, Cairo, Egypt.
[2]Saxony Egypt University for Applied Science and Technology, Egypt.

*Corresponding author(s). E-mail(s): moatazroshdy2015@mtc.edu.eg;

Abstract

This paper conducts a comprehensive analysis of the performance characteristics of Free Space Optical (FSO) communications systems operating across diverse channel conditions. The mathematical procedure for performance evaluation of single-input single-output (SISO) FSO is reviewed for versatile link position and direction, which facilitate for the beginner researchers starting the study of the physical FSO communications links from one article. Furthermore, We study a receiver-diversity arrangement consisting of a central aperture surrounded by a ring of apertures. Depending on this arrangement, the multiple-input multiple-output FSO performance is elaborated under various atmospheric turbulence and pointing error channel models for coherent and subcarrier intensity modulation systems. This MIMO-FSO arrangement can be used in the future to improve the system performance and reliability. Leveraging the $\boldsymbol{\alpha}$-$\boldsymbol{\mu}$ distribution and the proposed receiver configuration, we develop approximate analytical formulations for both the probability density function (PDF) of the instantaneous signal-to-noise ratio (SNR) and its corresponding cumulative distribution function (CDF). In the case of MIMO links with turbulence that is independent across apertures and pointing jitter common to all apertures, the outage probability and the ergodic capacity of the maximum ratio combining (MRC) and equal gain combining (EGC) are also formulated for MIMO-FSO systems in terms of the Fox-H

function and other simple functions. The performance gaps between different combining and modulation techniques are illustrated.

Keywords: Optimal combining (OC), suboptimal combining (SOC), equal gain combining (EGC), maximum ratio combining (MRC), maximum likelihood combining (MLC), ergodic capacity (EC), multiple-input multiple-output free-space optical (MIMO-FSO), Outage Probability (OP), gamma-gamma distribution (GG), and modulated-gamma distribution (MG)

1 Introduction

Free-space optical (FSO) communication is increasingly recognized as a promising technology, largely because of its capacity for high-speed data transmission, inherent communication security, and resilience to electromagnetic interference [1]. The escalating requirements for high-bandwidth, low-delay connectivity, driven by the advent of 5G and subsequent network generations, coincide with significant financial constraints. The substantial capital investment required for civil works—including excavation and subsequent land remediation—impedes the pervasive deployment of conventional optical fiber networks. In this context, FSO communication has arisen as a formidable technological solution, well-positioned to address these pressing connectivity needs [2]. FSO communication transmits data through the atmosphere via optical beams, presenting a compelling substitute for conventional RF systems [3, 4]. Its advantages include minimal latency, resilience to noise and electromagnetic interference, efficient spatial reuse, straightforward installation, and operation in a license-free spectrum. Furthermore, FSO provides enhanced security, alleviates spectrum scarcity, and supports exceptionally high data-rate transmissions between terminals over distances ranging from a few meters (terrestrial links) to thousands of kilometers (space links), demonstrating a substantial operational range [5]. FSO systems provide distinct benefits for line-of-sight (LoS) applications, establishing connections in scenarios where conventional fiber optic or RF links are impractical. A key feature is their use of highly directional, narrow laser beams. This focused transmission enables significant spatial reuse and inherently improves security by complicating interception efforts. The fundamental use of light as the signal carrier also provides inherent immunity to electromagnetic interference. The deployment of FSO systems is notably straightforward, and they can be relocated without the substantial expenses tied to permanent, dedicated fiber optic infrastructure. Furthermore, FSO technology operates at optical frequencies (hundreds of THz, e.g., the 850 nm and 1550 nm windows), a spectrum that requires no licence, thereby removing spectrum licensing fees (laser-safety regulations still apply) [6–8].

Spatial diversity is one of the most effective techniques for mitigating the impact of atmospheric turbulence (AT) and fading in FSO links. In single-input single-output (SISO) systems, performance significantly deteriorates under strong turbulence without using promising techniques like dynamic beam waist adjustment [9], often failing to satisfy bit-error-rate (BER) requirements within practical signal-to-noise ratio

(SNR) ranges [10]. While methods such as error-control coding (ECC) with interleaving [11, 12] and maximum-likelihood sequence detection (MLSD) [13, 14] have been explored, they typically incur drawbacks such as large interleaver sizes, high latency, and increased computational complexity [15, 16]. In contrast, spatial diversity provides a more practical and hardware-based approach, relying on multiple transmitters (Txs), receivers (Rxs), or both to reduce the severity and duration of deep fades, while also mitigating temporal blockage in dynamic environments [17, 18].

Spatial diversity can be realized in three principal configurations: multiple-input single-output (MISO), single-input multiple-output (SIMO), and multiple-input multiple-output (MIMO).

- **MISO systems** employ multiple transmit lasers that send the same signal toward a single detector. Repetition coding (RC) is the most common scheme and has been shown to outperform space–time block codes (STBC) and orthogonal designs in FSO channels [6, 19, 20].
- **SIMO systems** utilize multiple receive apertures. Here, combining strategies such as maximum ratio combining (MRC), equal gain combining (EGC), and selection combining (SC) are adopted. MRC provides the best SINR performance, while EGC offers a favorable trade-off between complexity and gain [21–23].
- **MIMO systems**, inspired by radio-frequency (RF) communications, extend these benefits by employing multiple Txs and Rxs simultaneously, enhancing capacity and turbulence resilience. However, performance can degrade due to spatial correlation when apertures are placed too close to one another [24, 25].

Overall, spatial diversity enhances link robustness by exploiting multiple independent optical paths, with performance gains scaling with the number of apertures [26]. Among the available techniques, **receiver diversity** (e.g., multiple lenses or apertures) is widely regarded as the simplest and most cost-efficient option [27]. When channel state information (CSI) is available, more advanced strategies such as transmit selection diversity (TSD) [28] and feedback-assisted beam forming [29] can be employed to further boost reliability.

Both experimental demonstrations and theoretical analyses confirm that spatial diversity remains a cornerstone of reliable and high-capacity FSO systems, particularly under strong turbulence conditions. Consequently, it constitutes a vital component in safeguarding the reliability and resilience of next-generation optical wireless networks [30–32].

The remainder of this paper is arranged as follows. In section 2, the channel models are introduced. The performance analysis of SISO-FSO systems is reviewed in section 3. In section 4, the performance metrics of MIMO-FSO systems are derived and numerical results are discussed. At the end, the conclusion and future work is given in section 5.

2 Channel Models

Before beginning our study, we have to discuss two major effects deteriorate the FSO system performance which are atmospheric turbulence (h_{at}) and pointing errors (h_p)

where the channel state (h) is proportional to the multiplication of them. The channel state $h = h_\ell h_{\text{at}} h_{\text{p}}$ models the random attenuation of the propagation channel. h arises due to three factors: path loss h_ℓ, pointing errors h_{p}, and atmospheric turbulence h_{at}. h_ℓ is constant over the propagation path, and both h_{p} and h_{at} are random with statistics discussed in Sections 2.1 and 2.2 respectively. The channel state is a product of two random variables so, the probability density function of the channel state can be expressed as

$$f_h\left(h; W_L\right) = \int f_{h|h_{\text{at}}}\left(h \mid h_{\text{at}}\right) f_{h_{\text{at}}}\left(h_{\text{at}}\right) dh_{\text{at}} \tag{1}$$

where $f_h\left(h; W_L\right)$ is a family of pdfs parameterized by the beam width at the receiver W_L and $f_{h|h_{\text{at}}}\left(h \mid h_{\text{at}}\right)$ is the conditional probability of state h given a turbulence state h_{at}. It should keep in mind that the value of h_ℓ is a deterministic scaling factor (path loss factor).

2.1 Pointing Errors effect

Pointing precision is a key factor in determining link performance and reliability in line-of-sight FSO communication links. Wind loads and thermal expansions, on the other hand, produce unpredictable building sways, which cause pointing mistakes resulting in signal fading at the receiver. In this part, we review a probabilistic model for pointing error loss owing to misalignment that takes detector aperture size, beam width, and jitter variance into account [33]. The normalized spatial distribution of the transmitted intensity at a distance L from the emitter for a Gaussian beam is given by [34].

$$I_{\text{beam}}\left(\boldsymbol{\rho_v}; L\right) = \frac{2}{\pi W_L^2} \exp\left(-\frac{2\|\boldsymbol{\rho_v}\|^2}{W_L^2}\right) \tag{2}$$

where $\boldsymbol{\rho_v}$ is the radial vector from the beam's centre and W_L is the beam radius (at the $1/e^2$ intensity level) at distance L. The beam waist W_L of a Gaussian beam moving through a turbulent atmosphere can be estimated as [35].

$$W_L \approx W_o \left[1 + \chi\left(\frac{\lambda L}{\pi W_o^2}\right)^2\right]^{\frac{1}{2}} \tag{3}$$

where W_o is the beam waist at $L = 0$, $\chi = 1 + 2W_o^2/\rho_o^2(L)$ and $\rho_o(L) = \left(0.55 C_n^2 k^2 L\right)^{-3/5}$ is the spherical-wave coherence length. Figure (1) shows a circular detecting aperture with radius a and a Gaussian beam shape at the receiver I_{beam}.

The loss caused by geometric spread with a pointing mistake of r based on the uncovered surface of the detector with certain area χ is written as

$$h_{\text{p}}(\boldsymbol{r}; L) = \int_{\chi} I_{\text{beam}}\left(\boldsymbol{\rho_v} - \boldsymbol{r}; L\right) d\boldsymbol{\rho_v} \tag{4}$$

where $h_{\text{p}}(\cdot)$ is the amount of power that the detector picked up, A is the detector area, and the relation $\chi \leq A$ always holds. When there is a pointing mistake of r, h_{p} depends on the angle and radial movement. Because of the symmetry of the beam

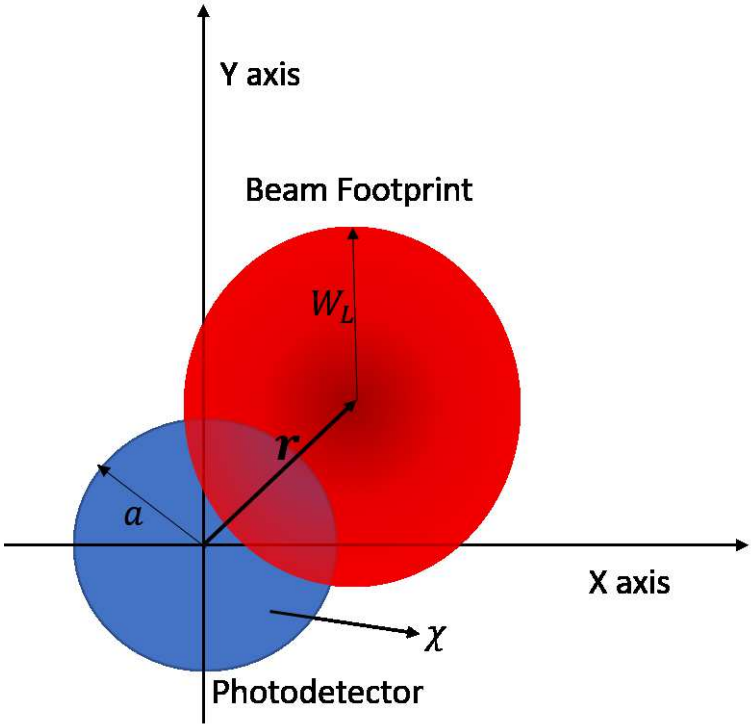


Fig. 1: Radial shift causing pointing errors.

form and detector area, the resulting $h_{\mathrm{p}}(\boldsymbol{r}; L)$ is only dependent on the radial distance $r = \|\boldsymbol{r}\|$. As a result, we may assume that the radial distance is positioned along the x-axis without losing generality. The proportion of collected power at a receiver of radius a in the incident wave's transverse plane may be represented as [36]

$$h_{\mathrm{p}}(r; L) = \int_{-a}^{a} \int_{-\eta_a}^{\eta_a} \frac{2}{\pi W_L^2} \exp\left(-2\frac{(x-r)^2 + y^2}{W_L^2}\right) dydx \tag{5}$$

where $\eta_a = \sqrt{a^2 - x^2}$. This integration can be approximated as the Gaussian form and the approximation is close to the exact, as shown in Figure (2) [36].

$$h_{\mathrm{p}}(r; L) \approx A_0 \exp\left(-\frac{2r^2}{W_{Leq}^2}\right) \tag{6}$$

where $v = (\sqrt{\pi}a)/\left(\sqrt{2}W_L\right)$, $A_0 = [\mathrm{erf}(v)]^2$ and $W_{Leq}^2 = W_L^2 \frac{\sqrt{\pi}\,\mathrm{erf}(v)}{2v\exp(-v^2)}$.

A_0 is the proportion of gathered power at $r = 0$, and W_{Leq} is the equivalent beam width. As in prior work, consider of independent identical Gaussian distributions for vertical and horizontal displacement. A Rayleigh distribution is used to describe the

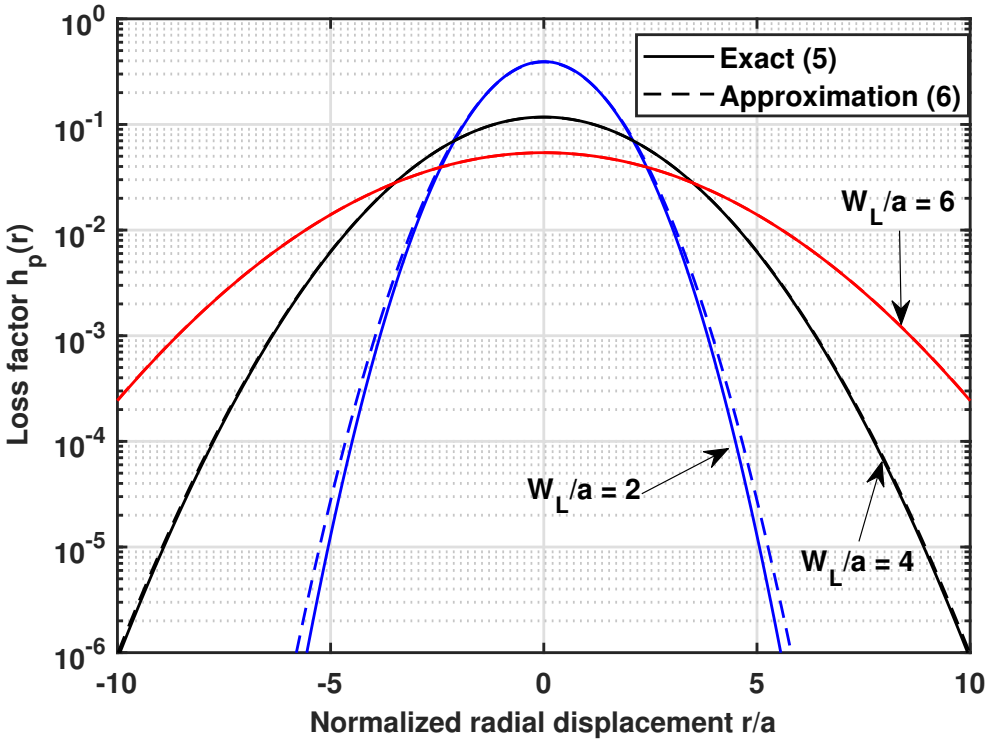


Fig. 2: The relation between pointing loss factor and normalized radial shift.

radial displacement r at the receiver.

$$f_r(r) = \frac{r}{\sigma_s^2} \exp\left(-\frac{r^2}{2\sigma_s^2}\right), \quad r > 0 \tag{7}$$

where σ_s^2 is the amount of variations in the jitter at the receiver. By combining equations (6) and (7), one can formulate an expression for the probability distribution of h_p [36].

$$f_{h_\mathrm{p}}(h_\mathrm{p}) = \frac{\delta^2}{A_0^{\delta^2}} h_\mathrm{p}^{\delta^2-1}, \quad 0 \le h_\mathrm{p} \le A_0 \tag{8}$$

where $\delta = W_{Leq}/2\sigma_s$ is the ratio between the equivalent beam radius and the pointing error displacement standard deviation at the receiver and the corresponding mean of h_p is $E(h_p) = \frac{\delta^2 A_0}{\delta^2+1}$.

2.2 Atmospheric Turbulence Effect

Atmospheric turbulence fading coefficient h_{at} is a parameter which is coming from random fluctuations in pressure and temperature causing optical impairments making small and large turbulent eddies as shown in Figure (3). The small turbulent eddies are

the dominant in Figure (3a) with diffraction nature. In contrast, the large turbulent eddies are the dominant in Figure (3b) with refraction nature. These fluctuations cause changes in the received signal's amplitude and phase, resulting in system deterioration. This random process can be well represented by using known weather parameters for horizontal (for example: building to building link) or vertical path (for example: ground to satellite link). Consequently, we can say that in each FSO link there is a turbulence model which produces an accurate results.

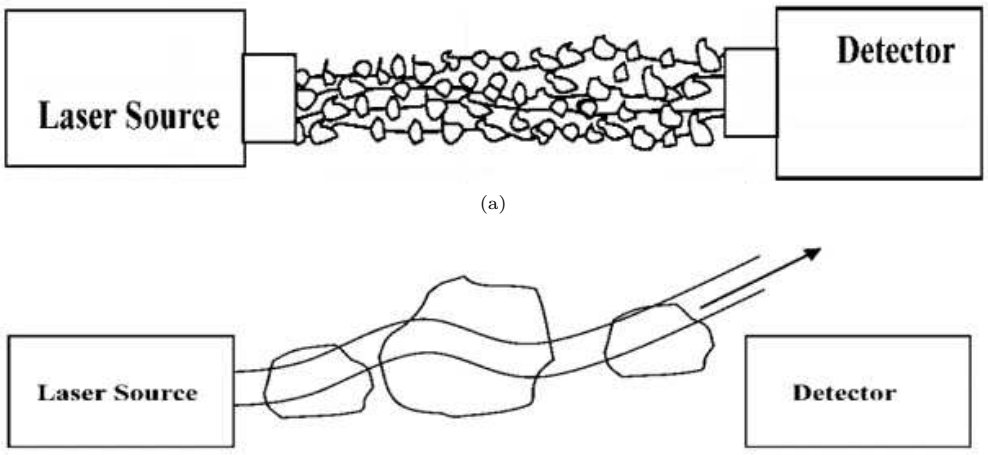


Fig. 3: (a) Weak turbulence resulting in optical scintillation, (b) Strong turbulence resulting in beam wandering.

Horizontal Path: In most terrestrial links such as communication links between two buildings, the propagation path is considered as a horizontal path. The Log-normal (LN) and Gamma-Gamma (GG) distributions are the most famous models used in this type of links to characterize the atmospheric turbulence in weak and strong turbulence regimes respectively with probability density functions ($f_{h_{at}}(h_{at})$) given as follows [37, 38].

$$f_{h_{\mathrm{at}}}\left(h_{\mathrm{at}}\right)=\frac{1}{2h_{\mathrm{at}}\sqrt{2\pi\sigma_X^2}}\exp\left(-\frac{\left(\ln h_{\mathrm{at}}+2\sigma_X^2\right)^2}{8\sigma_X^2}\right). \tag{9}$$

$$f_{h_{at}}(h_{at})=\frac{2(\rho_1\rho_2)^{(\rho_1+\rho_2)/2}}{\Gamma(\rho_1)\Gamma(\rho_2)}h_{at}^{\frac{\rho_1+\rho_2}{2}-1}k_{\rho_1-\rho_2}(2\sqrt{\rho_1\rho_2 h_{at}}) \tag{10}$$

where σ_X^2 is log-amplitude variance, $\Gamma(.)$ is the gamma function, $k_x(y)$is the modified Bessel function of the second type, and $1/\rho_1$ and $1/\rho_2$ are the variances of the small

and large scale eddies[1] given by

$$\rho_1 = \frac{1}{\exp\left[\frac{0.49\sigma_R^2}{\left(1+1.11\sigma_R^{12/5}\right)^{7/6}}\right] - 1} \tag{11}$$

$$\rho_2 = \frac{1}{\exp\left[\frac{0.51\sigma_R^2}{\left(1+0.69\sigma_R^{12/5}\right)^{5/6}}\right] - 1} \tag{12}$$

where, σ_R^2 is the Rytov variance which is given as follows:

$$\sigma_R^2 = 1.23 C_n^2(z) k^{7/6} L^{11/6} \approx 4\sigma_X^2 \tag{13}$$

where $C_n^2(z)$ denotes the index of refraction structural parameter at height z (assumed constant over the route in the equations below; see the remark following them for non-uniform profiles), and $k = 2\pi/\lambda$ denotes the optical wave number. For horizontal link, the GG pdf has been driven to fulfill with measurements under a range of turbulence situations [43]. For a slant path with non-uniform $C_n^2(h)$ the plane-wave Rytov variance is $\sigma_R^2 = 2.25k^{7/6}\int_0^L C_n^2(h(s))(L-s)^{5/6}ds$, with s measured from the transmitter and $h(s) = Z_{tx} \mp s\cos\psi$; it reduces to $1.23C_n^2k^{7/6}L^{11/6}$ for constant C_n^2, so the constant value used here is a path-effective one, $C_{n,\text{eff}}^2 = \sigma_R^2/(1.23k^{7/6}L^{11/6})$. For the Hufnagel–Valley profile with the nominal ground-level strength $A = 1.7\times10^{-14}$ m$^{-2/3}$, C_n^2 varies from 2.2×10^{-16} to 2.5×10^{-15} along the 200–600 m link, and $C_{n,\text{eff}}^2 = 0.5\times10^{-15}$ (transmitter at the upper UAV) or 1.0×10^{-15} (lower UAV), i.e. $\sigma_R^2 = 0.013$ and 0.028, which is weaker than our weak case. The three values of Table 3 are therefore to be read as path-effective scenarios (equivalent to ground-level strengths $A \approx 2.8\times10^{-13}$, 1.2×10^{-12} and 5.9×10^{-12} m$^{-2/3}$ for the HV shape); the profile integral is provided in the accompanying MATLAB code. The plane-wave ρ_1, ρ_2 above are consistent with the plane-wave σ_R^2, and the beam shape enters only through the pointing-error loss.

Vertical Path (Ground to Satellite Link): For ground to satellite link, the Modulated Gamma (MG) had provided an excellent fit with the simulation results from the Lincoln laboratory numerical wave optics code [44] and experimental data [45].

$$f_{h_{at}}(h_{at}) = \frac{b_w}{\Gamma(\nu)h_{at}} G_{1,2}^{2,0}\left[\frac{b_w\nu h_{at}}{(1+b_w)\bar{h}_a}\Bigg|_{b_w,\nu}^{1+b_w}\right], \quad h_{at} \geq 0 \tag{14}$$

where b_w is the beam-wander parameter, ν is the shape parameter of the gamma distribution, and $\bar{h}_a$ is the mean value of h_{at}.

[1] It is noted that the parameters ρ_1 and ρ_2 vary depending on the wave propagation model [39]. Hence, they can be determined from the Rytov variance [40–42].

2.3 Combined effect

By using the pointing errors probability density functions (8) stated previously, The conditional probability distribution given a turbulence state h_{at} is obtained as [36]

$$\begin{aligned} f_{h|h_{\text{at}}}\left(h \mid h_{\text{at}}\right) &= \frac{1}{h_{\text{at}} h_\ell} f_{h_{\text{p}}}\left(\frac{h}{h_{\text{at}} h_\ell}\right) \\ &= \frac{\delta^2}{A_0^{\delta^2} h_{\text{at}} h_\ell}\left(\frac{h}{h_{\text{at}} h_\ell}\right)^{\delta^2-1}, \quad 0 \le h \le A_0 h_{\text{at}} h_\ell \end{aligned} \tag{15}$$

where $\delta = W_{Leq}/2\sigma_s$ is the ratio between the equivalent beam radius and the pointing error displacement standard deviation at the receiver and A_0 is the proportion of gathered power when the detector and beam footprint are coincide. Substituting by (15) into (1), we get

$$f_h\left(h; W_L\right) = \frac{\delta^2}{\left(A_0 h_\ell\right)^{\delta^2}} h^{\delta^2-1} \int_{h/A_0 h_\ell}^{\infty} h_{\text{at}}^{-\delta^2} f_{h_{\text{at}}}\left(h_{\text{at}}\right) dh_{\text{at}} \tag{16}$$

By using the turbulence probability density functions which are path dependent, we can get full description for the channel fading in terrestrial link (upper term in equation (17)) [46] by using equation (10) and satellite uplink (lower term in equation (17)) [47] by using equation (14).

$$f_h(h) = \begin{cases} \frac{\rho_1 \rho_2 \delta^2}{A_o h_l \Gamma(\rho_1)\Gamma(\rho_2)} G_{1,3}^{3,0}\left[\frac{\rho_1 \rho_2 h}{A_o h_l}\middle|_{\delta^2-1,\rho_1-1,\rho_2-1}^{\delta^2}\right], & h \ge 0 \\ \frac{\delta^2 b_w}{\Gamma(\nu) h_l h} G_{2,3}^{3,0}\left[\frac{b_w \nu h}{(1+b_w) h_l \bar{h}_a A_0}\middle|_{\delta^2, b_w, \nu}^{1+b_w, 1+\delta^2}\right], & h \ge 0 \end{cases} \tag{17}$$

where b_w is the beam-wander parameter, ν is the shape parameter of the gamma distribution, $\bar{h}_a$ is the mean value of h_{at}, $1/\rho_1$ and $1/\rho_2$ are the variances of the small and large scale eddies, $\Gamma()$ is the gamma function, and $G_{a,b}^{c,d}$ is the Meijer-G function.

3 Performance Analysis of FSO systems

In this section, we study the channel capacity and outage probability, and the average symbol error rate ASER including the latest studies only [47, 48] besides the validation of the mathematical expression using Monte Carlo (MC) Simulation. In table (1), a research works about SISO-FSO channel modeling are introduced which consider the pointing errors effects.

3.1 SNR probability density function

The instantaneous SNR is γ_m where m is the mode of reception with $m = 1$ for coherent detection and $m = 2$ for direct detection. The coherent and direct detections SNR are $\gamma_1 = \gamma_{\text{coherent}} = C_c I$ and $\gamma_2 = \gamma_{\text{SIM/DD}} = C_s I^2$ respectively [55]. The receiver

Table 1: SISO-FSO work survey.

Ref.	Detection	Turbulence model
[33]	Direct	LN and GG (Numerical)
[49]	Coherent	EW
[50, 51]	Direct	LN and GG
[52]	Direct and Coherent	GG
[47, 53]	Direct and Coherent	MG
[48]	Direct and Coherent	GG
[54]	Direct	the exponentiated Weibull

irradiance can be normalized as $I = \bar{I}h$ where $\bar{I}$ is the average receiver irradiance then substitute in instantaneous SNR $\gamma_{\text{coherent}} = C_c\bar{I}h$ and $\gamma_{\text{SIM/DD}} = C_s(\bar{I}h)^2$. The mean SNRs of coherent and direct detection are $\bar{\gamma}_1 = \mathbb{E}[\gamma_1]$ and $\bar{\gamma}_2 = \mathbb{E}[\gamma_2]$ respectively, where m is the mode of reception with $m = 1$ for coherent detection and $m = 2$ for direct detection then $\bar{\gamma}_1 = C_c\bar{I}\mathbb{E}[h]$ and $\bar{\gamma}_2 = C_s\bar{I}^2\mathbb{E}[h^2]$ respectively [55]. From the previous equations, we can obtain after simple manipulation that $h = \sqrt[m]{\mathbb{E}[h^m]\gamma_m/\bar{\gamma}_m}$. The closed-form SNR statistics below follow [48, 55] and are written in terms of the normalised SNR ${\mu_m}^{2,3}$, i.e. the electrical SNR obtained for unit-mean turbulence irradiance ($\mathbb{E}[h_{\text{at}}] = 1$) and no pointing loss. It differs from the mean SNR by the pointing-loss factors in the moment expression below: for GG turbulence, $\bar{\gamma}_1 = \frac{\delta^2}{1+\delta^2}\mu_1$ and $\bar{\gamma}_2 = \frac{\delta^2(1+\rho_1)(1+\rho_2)}{(2+\delta^2)\rho_1\rho_2}\mu_2$.

By utilizing this simple random variable transformation, depending on h distribution the resulting SNR PDF under the coherent and direct detection techniques is obtained which is given for GG turbulent channel with pointing errors [48] using equation (17).

$$f_{\gamma_m}(\gamma_m) = \frac{\delta^2}{m\gamma_m\Gamma(\rho_1)\Gamma(\rho_2)}\mathrm{G}_{1,3}^{3,0}\left[\rho_1\rho_2\left(\frac{\gamma_m}{\mu_m}\right)^{\frac{1}{m}}\middle|\begin{matrix}\delta^2+1\\ \\ \delta^2,\rho_1,\rho_2\end{matrix}\right] \tag{18}$$

the moments are defined as $\mathbb{E}\left[\gamma^n\right]$ and given by [48]

$$\mathbb{E}\left[\gamma_m^n\right] = \frac{\delta^2\Gamma(mn+\rho_1)\Gamma(mn+\rho_2)}{(\rho_1\rho_2)^{mn}\left(mn+\delta^2\right)\Gamma(\rho_1)\Gamma(\rho_2)}\mu_m^n \tag{19}$$

[2]The parameter $\mu_1 = C_c$ represents the average SNR for coherent FSO systems under the condition of normalized irradiance (i.e., $\mathbb{E}[I] = 1$) [55]. Here, $C_c = 2R^2AP_{LO}/\left[2qR\Delta BP_{LO} + 2\Delta B\left(qRAI_b + 2k_bT_kF_n/R_L\right)\right] \approx RA/(q\Delta B)$ functions as a multiplicative constant specific to a given coherent system. This constant is defined by several physical parameters: R is the photodetector responsivity, A is the photodetector area, P_{LO} is the local oscillator power, ΔB is the receiver's noise equivalent bandwidth, q is the electronic charge, I_b is the background irradiance, k_b is Boltzmann's constant, T_k is the temperature in Kelvin, F_n is a thermal noise enhancement parameter, and R_L is the load resistance.

[3]$\mu_2 = C_s$ is the average SNR for SIM/DD FSO systems for unit-mean turbulence irradiance and no pointing loss (i.e., $\mathbb{E}[h_{\text{at}}] = 1$) [55] , where $C_s = (RA\xi)^2/\left[2\Delta B\left(qRAI_b + 2k_bT_kF_n/R_L\right)\right]$ is a multiplicative constant for a given SIM/DD system with modulation index ξ.

for MG turbulent channel with pointing errors [47] using equation (17).

$$f_{\gamma_m}(\gamma_m) = \frac{\delta^2 b_w}{m\Gamma(\nu)}\gamma_m^{-1} G_{2,3}^{3,0}\left[\frac{\delta^2 b_w \nu \left(\gamma_m/\mu_m\right)^{\frac{1}{m}}}{\left(1+b_w\right)\left(1+\delta^2\right)}\middle|_{\delta^2, b_w, \nu}^{1+b_w, 1+\delta^2}\right] \tag{20}$$

with the corresponding moments as follow

$$\mathbb{E}\left[\gamma_m^n\right] = \frac{\delta^2 b_w \Gamma(mn+\nu)\mu_m^n}{\left(mn+b_w\right)\left(mn+\delta^2\right)\Gamma(\nu)}\left[\frac{\left(1+b_w\right)\left(1+\delta^2\right)}{\delta^2 b_w \nu}\right]^{mn} \tag{21}$$

Depending on the SNR probability density function and the moments, we can calculate the outage probability, ASER, and ergodic capacity versus the average SNR as shown in the next sections.

3.2 Outage Probability

An outage condition occurs when the instantaneous output signal-to-noise ratio γ drops beneath a predefined threshold γ_{th}, making the analysis of outage probability (OP) a key system performance metric. A fundamental relationship to note is that the CDF of the instantaneous SNR γ is mathematically equivalent to the OP for an FSO channel. In other words, the outage probability is defined as the likelihood that the received SNR is less than the threshold γ_{th} necessary to maintain a specific quality of service (QOS). This can be formally expressed by

$$\mathrm{OP} = \int_0^{\gamma_{th}} f_\gamma(t)dt \tag{22}$$

for GG channel with pointing errors, OP is derived as [48]

$$\mathrm{OP} = A_{gg}\mathrm{G}_{m+1,3m+1}^{3m,1}\left[\left(\frac{B_{gg}}{\mu_m}\right)\gamma_{th}\middle|_{\kappa_2,0}^{1,\kappa_1}\right] \tag{23}$$

where $A_{gg} = \frac{m^{\rho_1+\rho_2-2}\delta^2}{(2\pi)^{m-1}\Gamma(\rho_1)\Gamma(\rho_2)}$, $B_{gg} = \frac{(\rho_1\rho_2)^m}{m^{2m}}$, $\kappa_1 = \frac{\delta^2+1}{m}, \ldots, \frac{\delta^2+m}{m}$ comprises of m terms, and $\kappa_2 = \frac{\delta^2}{m}, \ldots, \frac{\delta^2+m-1}{m}, \frac{\rho_1}{m}, \ldots, \frac{\rho_1+m-1}{m}, \frac{\rho_2}{m}, \ldots, \frac{\rho_2+m-1}{m}$ comprises of 3m terms. for MG channel with pointing errors, OP is derived as [47]

$$\mathrm{OP} = A_{mg}G_{2m+1,3m+1}^{3m,1}\left[\left(\frac{B_{mg}}{\mu_m}\right)\gamma_{th}\middle|_{\kappa_2,0}^{1,\kappa_1}\right] \tag{24}$$

where $A_{mg} = \frac{\delta^2 b_w m^{\nu-2.5}}{(2\pi)^{\frac{m-1}{2}}\Gamma(\nu)}$ $B_{mg} = \left(\frac{\delta^2 b_w \nu}{m(1+b_w)(1+\delta^2)}\right)^m$, $\kappa_1 = \frac{b_w+1}{m}, \ldots, \frac{b_w+m}{m}, \frac{\delta^2+1}{m}, \ldots, \frac{\delta^2+m}{m}$ with $2m$-terms, and $\kappa_2 = \frac{\delta^2}{m}, \ldots, \frac{\delta^2+m-1}{m}, \frac{b_w}{m}, \ldots, \frac{b_w+m-1}{m}, \frac{\nu}{m}, \ldots, \frac{\nu+m-1}{m}$ with $3m$-terms.

3.3 Ergodic Capacity

The increasing demand for wireless communication highlights the necessity of identifying the capacity limits of the channels that underlie these systems. These capacity limits determine the maximum data rates that may be communicated through wireless channels while maintaining an asymptotically small error probability. This is done under the assumption that there are no limitations on the latency or complexity of the encoder and the decoder. In the late 1940s, Shannon was a pioneer in developing the mathematical theory of communication that underpins the concept of channel capacity [56]. This theoretical framework is fundamentally built upon the concept of mutual information shared between a channel's input and its corresponding output. In contrast to the situation of additive white gaussian noise (AWGN), the capacity of a flat fading channel cannot be determined using a single formula. This is due to the fact that capacity is dependent on the information that is known about the time-varying channel at the transmitter and/or receiver. In addition, depending on the channel information assumptions that are made, various definitions of channel capacity can be used. These definitions differ according to whether capacity is defined as the maximum rate that is averaged over all fading states or as the maximum constant rate that can be maintained in all states of fading (with or without some outage probability). In a nutshell, the channel capacity depends on what is known about the channel state information (CSI)at the terminals. There are three different Perspectives considering this knowledge as follows.

1. Channel distribution information (CDI): The distribution of the channel state is known to the transmitter and receiver.
2. Receiver CSI: The value of the channel state is known to the receiver simultaneously, and CDI holds too.
3. Transmitter and receiver CSI: The value of the channel state is known to the transmitter and receiver simultaneously, and both know the CDI.

The first scenario is intricate to do, the second have two definition of capacity which are ergodic capacity (EC) and capacity with outage.The ergodic capacity well be covered in this section and section 4.4. Finally, the third scenario will be taken into account in our future work.

Moreover, it is necessary to state that FSO channel is a slow fading channel, so the capacity achieving code is long enough to expose all channel states resulting in significant delay. For delay-constrained operation the relevant measure is the capacity with outage, $C_{\text{out}}(P_{\text{out}}) = (1 - P_{\text{out}}) \log_2(1 + \gamma_{\text{th}})$, where the threshold γ_{th} satisfies $\mathrm{P}(\gamma < \gamma_{\text{th}}) = P_{\text{out}}$ (the target outage probability), reported for the MIMO link in Table 7. Moreover, $\log_2(1+\gamma)$ is the Shannon-type spectral efficiency of the equivalent electrical channel; it is used here as a comparative figure of merit and not as the exact IM/DD capacity. The normalized ergodic capacity (EC) $\bar{C}$ is defined as $\bar{C} \triangleq \mathbb{E}\left[\log_2(1+\gamma)\right]$. By averaging this equation over (18) or (20). To put the previous integral in standard form we use the rules $\log_n(x) = \ln(x)/\ln(n)$ and $\ln(1+x) = G_{2,2}^{1,2}\left[x \mid \begin{matrix} 1,1 \\ 1,0 \end{matrix}\right]$. Then applying equation [07.34.21.0011.01] in [57], we have (25) and (26) for GG and MG channels repectively with corresponding vectors κ_1 and κ_2 [47,

48].

$$\bar{C} = \frac{A_{gg}}{\ln(2)} G_{m+2,3m+2}^{3m+2,1}\left[\frac{B_{gg}}{\mu_m}\Big|_{\kappa_2,0,0}^{0,1,\kappa_1}\right] \tag{25}$$

$$\bar{C} = \frac{A_{mg}}{\ln(2)} G_{2m+2,3m+2}^{3m+2,1}\left[\frac{B_{mg}}{\mu_m}\Big|_{\kappa_2,0,0}^{0,1,\kappa_1}\right] \tag{26}$$

3.4 Average SER

The average symbol error rate (ASER) is determined by integrating the conditional symbol error probability $P_e(\gamma)$ across the PDF of the SNR.

$$ASER = \int_0^\infty P_e(\gamma) f_{\gamma_{FSO}}(\gamma) d\gamma \tag{27}$$

The chosen digital modulation strategy affects the expression of P_c. Here, we concentrate on the binary phase shift keying (BPSK), M-PSK, and square M-QAM, where $P_e(\gamma) = \mathcal{C}_{mod}\,\text{erfc}\,\sqrt{\mathcal{D}_{mod}\gamma}$ and the differential BPSK (DBPSK), where $P_e(\gamma) = \mathcal{C}_{mod}\exp(-\mathcal{D}_{mod}\gamma)$, where the parameters $\mathcal{C}_{mod}$ and $\mathcal{D}_{mod}$ are provided in table (2).

Table 2: $\mathcal{C}_{mod}$ and $\mathcal{D}_{mod}$ parameters. The first three rows use $P_e = \mathcal{C}_{mod}\,\text{erfc}\,\sqrt{\mathcal{D}_{mod}\gamma}$ (BPSK: $\frac{1}{2}\,\text{erfc}\,\sqrt{\gamma}$); DBPSK uses $P_e = \mathcal{C}_{mod}e^{-\mathcal{D}_{mod}\gamma} = \frac{1}{2}e^{-\gamma}$, so equal numerical values refer to different functional forms.

Modulation Scheme	$\mathcal{C}_{mod}$	$\mathcal{D}_{mod}$	M
BPSK (erfc form)	1 / 2	1	-
M -PSK	1	$\sin^2(\pi/M)$	> 4
square M -QAM	2-2 / $\sqrt{M}$	3/(2(M-1))	≥ 4
DBPSK (exponential form)	1 / 2	1	-

3.4.1 ASER for BPSK, M -PSK and M -QAM

To depict $\text{erfc}(\sqrt{x})$ as the Meijer-G function describes $\text{erfc}(\sqrt{x}) = \frac{1}{\sqrt{\pi}} G_{1,2}^{2,0}\left[x|_{0,1/2}^{1}\right]$ and then using equation [07.34.21.0011.01] in [57], the unified expression for ASER is given by

$$ASER = \frac{\mathcal{C}_{mod}A_{mg}}{\sqrt{\pi}} G_{2m+2,3m+1}^{3m,2}\left[\frac{B_{mg}}{\mathcal{D}_{mod}\mu_m}\Big|_{\kappa_2,0}^{1,1/2,\kappa_1}\right]. \tag{28}$$

for the MG channel. For the GG channel the same steps give, with A_{gg}, B_{gg}, κ_1 (m terms) and κ_2 ($3m$ terms) as defined for the GG outage probability (checked numerically against direct integration of the GG SNR pdf for $m = 1, 2$),

$$ASER = \frac{\mathcal{C}_{mod}A_{gg}}{\sqrt{\pi}} G_{m+2,3m+1}^{3m,2}\left[\frac{B_{gg}}{\mathcal{D}_{mod}\mu_m}\Big|_{\kappa_2,0}^{1,1/2,\kappa_1}\right]. \tag{29}$$

3.4.2 ASER for DBPSK

By using equation [07.34.03.0228.01] in [57] to represent $\exp(-x)$ in terms of the Meijer-G function as $\exp(-x) = G_{0,1}^{1,0}\left[x \mid \begin{matrix} - \\ 0 \end{matrix}\right]$ and then using equation [07.34.21.0011.01] in [57], the unified expression for ASER is given by

$$ASER = \mathcal{C}_{mod} A_{mg} G_{2m+1,3m}^{3m,1}\left[\frac{B_{mg}}{\mathcal{D}_{mod}\mu_m}\middle|_{\kappa_2}^{1,\kappa_1}\right]. \tag{30}$$

for the MG channel, and for the GG channel

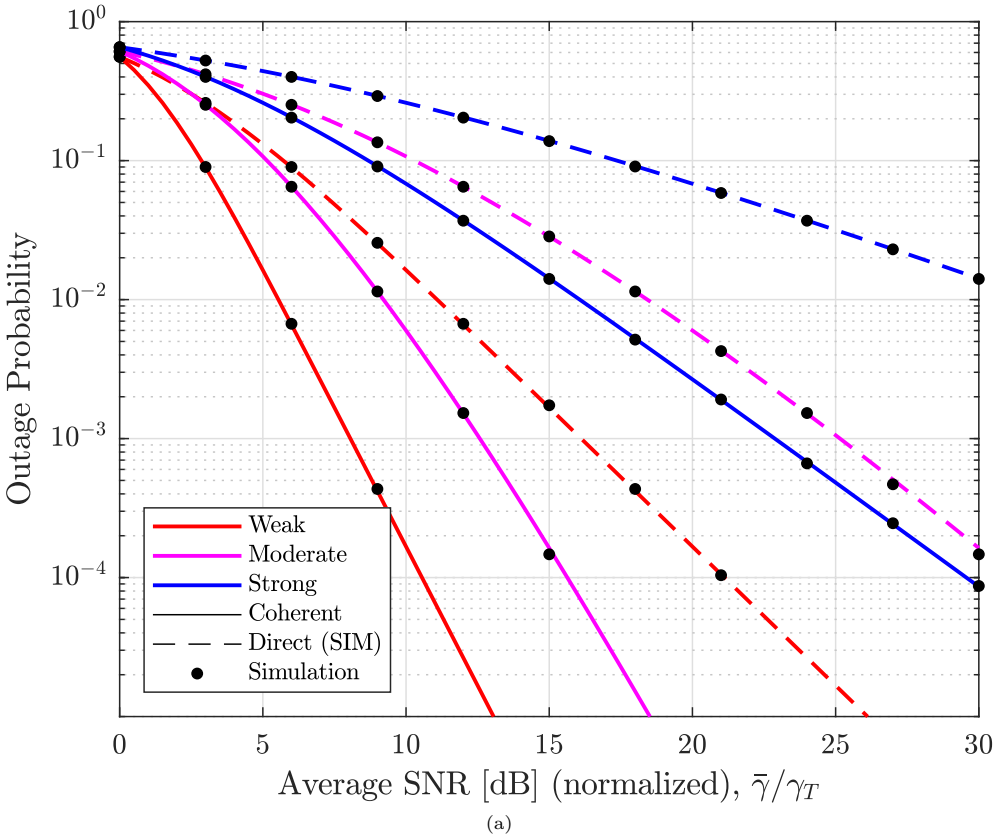
$$ASER = \mathcal{C}_{mod} A_{gg} G_{m+1,3m}^{3m,1}\left[\frac{B_{gg}}{\mathcal{D}_{mod}\mu_m}\middle|_{\kappa_2}^{1,\kappa_1}\right]. \tag{31}$$

3.5 Numerical Results of FSO Systems

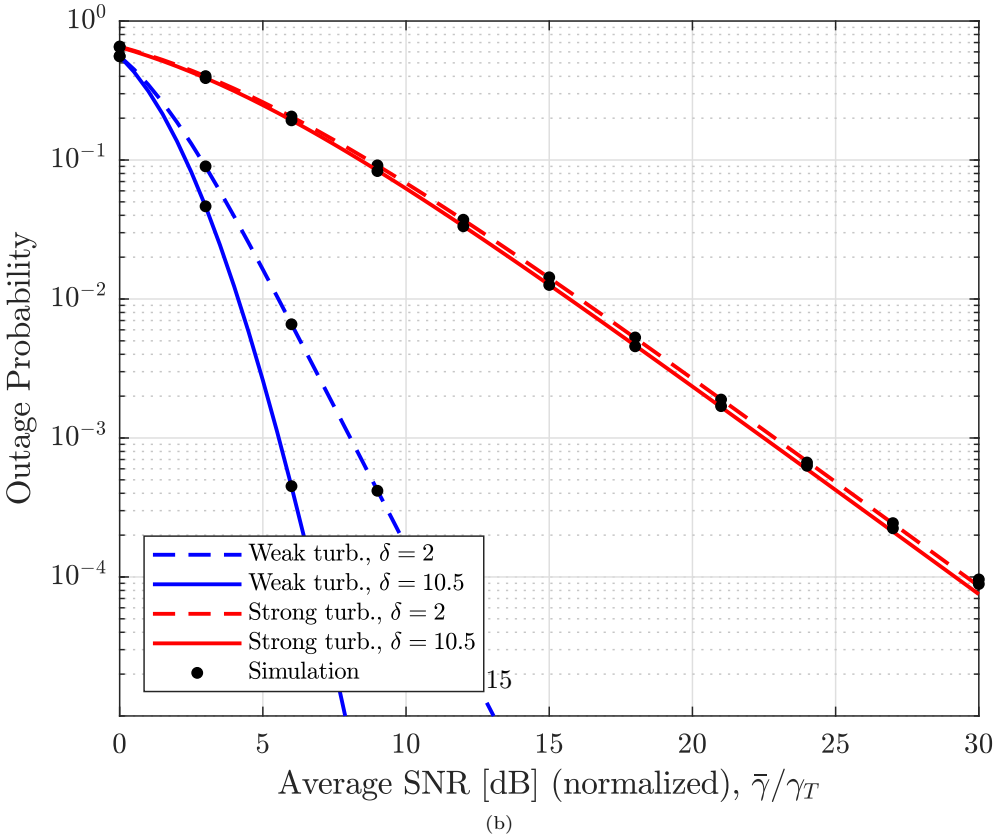
As an illustration of the mathematical formula presented above, simulation results for different performance metrics of a single FSO link transmission system is presented in this section by using link configurations in Table (3) as a default parameters of the system. Figure (4) shows the outage probability of FSO channel under operation of coherent and direct detection techniques. It is demonstrated that the atmospheric turbulence conditions gets severe and/or the pointing error, the outage probability increases and the ergodic capacity decreases. The pointing errors effect in strong turbulence becomes smaller than the effect in weak turbulence condition. The simulation results are obtained by using MATLAB from now and on-words. In this section the horizontal axis is the normalised SNR μ_m defined in Sec. 3.1; the mean SNR is lower by the pointing-loss factors given there. In the MIMO section every scheme is plotted versus its own mean SNR $\bar{\gamma} = \mathbb{E}[\gamma]$.

Table 3: FSO link parameters.

Parameter	**Symbol**	**Value**
Transceiver at high altitude settings	Z_{u1}	600 m
Transceiver at low altitude settings	Z_{u2}	200 m
Angle between the link and the vertical	ψ	70^o
Rytov variance (plane wave)	σ_R^2	0.13, 0.53, 2.65
Threshold SNR	γ_T	3 dB
Diameter of receiving aperture	$2a$	10 cm
Diameter of transmitting aperture	D_T	10 cm
Transceiver position standard deviation	σ_p	10 cm
Transceiver orientation standard deviation	σ_ψ	1×10^{-6}
Index of refraction structure parameter	C_n^2	$[5 \times 10^{-15} - 1 \times 10^{-13}]$
Optical wavelength	λ	1550×10^{-9} m
Beam divergence angle	θ_{div}	2 $mrad$
Ring radius of the receivers	$\mathbb{R}_{crl}$	$3a = 15$ cm
Gauss-Laguerre nodes	c	100

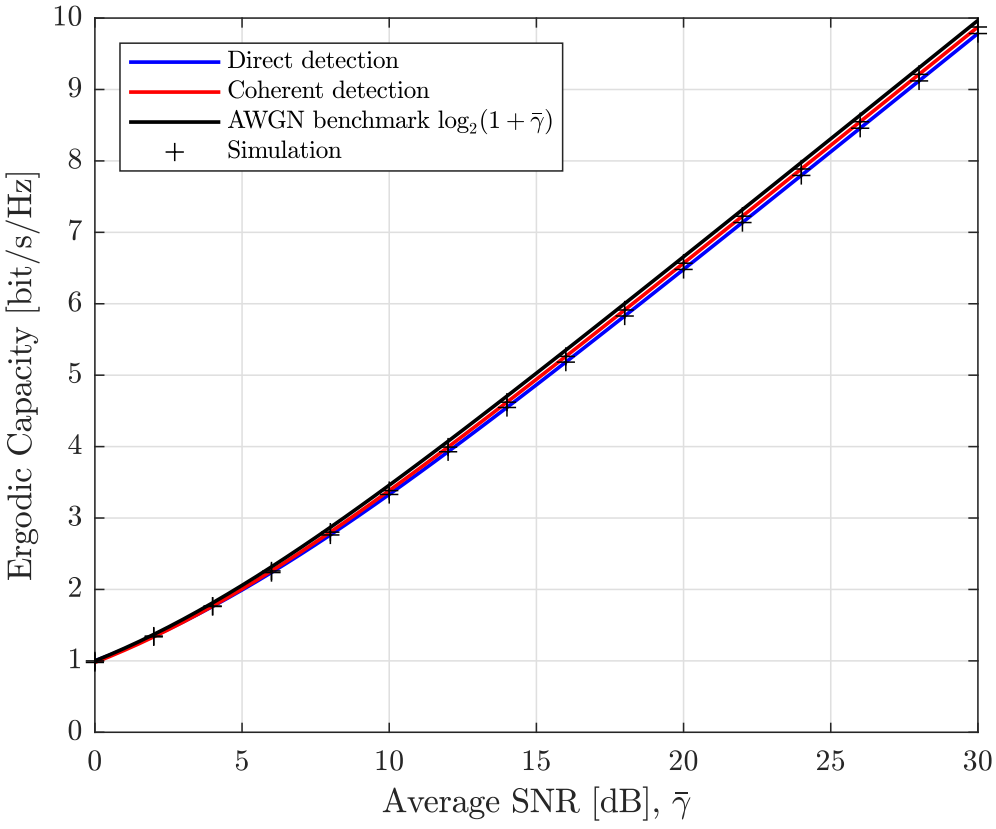


(a)

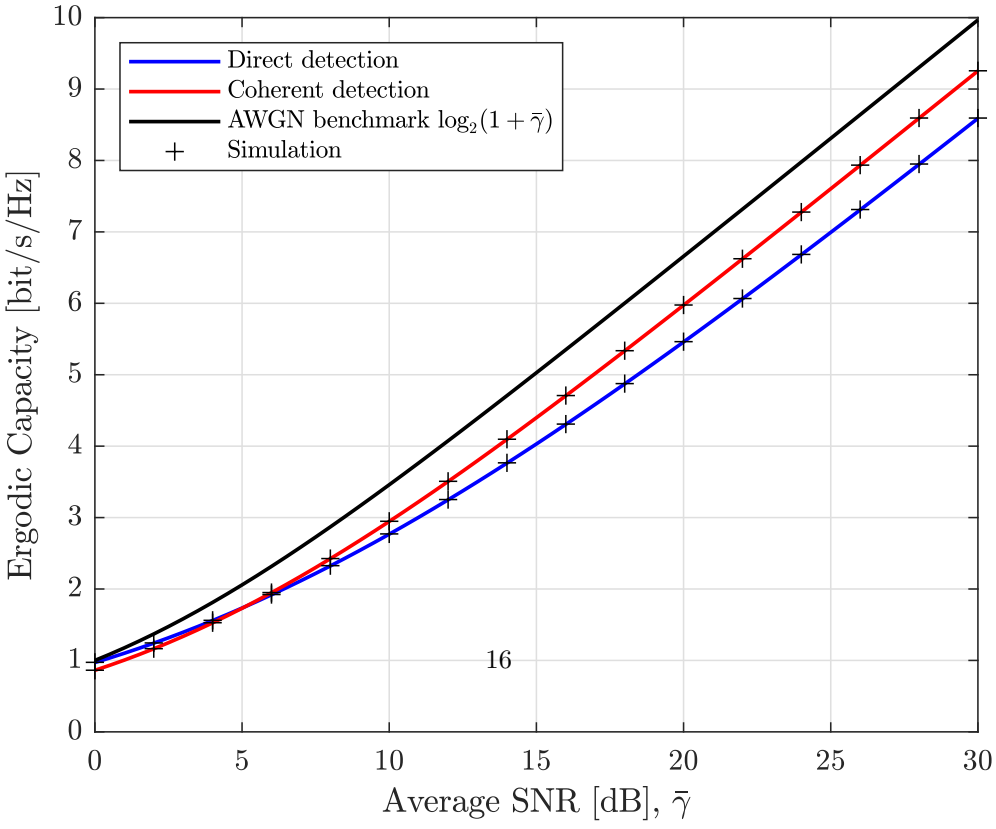


(b)

Fig. 4: Outage probability of the horizontal link versus the normalized SNR $\bar{\gamma}/\gamma_T$: (a) coherent (solid) and direct/SIM (dashed) detection under weak, moderate and strong turbulence ($\delta \approx 8.4$); (b) coherent detection for $\delta = 2$ and $\delta = 10.5$ under weak and strong turbulence. Markers: Monte Carlo simulation; the direct-detection SNR is normalized as in the SISO analysis, $\mu h^2/\mathbb{E}[h]^2$.



(a)



(b)

Fig. 5: Ergodic Capacity of horizontal link versus the average SNR (a)Weak turbulent channel with pointing error, (b) Strong turbulent channel with pointing error. The black curve is the AWGN benchmark $\log_2(1+\bar{\gamma})$, an upper bound on the ergodic capacity by Jensen inequality.

Finally, Figure (5) shows that the distance between the ergodic capacity of coherent detection and the AWGN benchmark $\log_2(1+\bar{\gamma})$ in strong turbulence is roughly seven times the distance in weak turbulence (about 0.5 versus 0.075 bit/s/Hz at 10 dB, and 0.69 versus 0.09 bit/s/Hz at 20 dB). In the next section, we show that spatial diversity narrows this gap for both coherent and SIM/DD systems.

4 Performance Analysis of Enhanced FSO systems Using Spatial Diversity (MIMO)

In table (4), a brief about MIMO-FSO channel modeling is introduced. The major studies take into account the pointing errors rising from random position fluctuations without considering random orientations which exist in airborne systems. In our study, we will take all scenarios causing pointing errors.

Table 4: MIMO-FSO work survey.

Ref.	Combining methods	Turbulence model	Pointing errors
[58]	OC-EGC	LN	-
[59]	SC	LN	-
[24]	OC-EGC	LN and Rayleigh,	-
[60]	MLC-SOC	LN and Neg. Exp	-
[20]	Alamouti	GG	
[61]	EGC-MRC	GG	Considered
[62]	EGC	LN	Considered
[63]	OSM/MLD	LN, GG, and Neg. Exp	Considered

4.1 Link Configuration

The analysis involves a slanted communication link connecting two hovering transceivers positioned at altitudes Z_{u1} and Z_{u2}, with the condition that $(Z_{u1} \geq Z_{u2})$. Both of the transceivers are equipped with lightweight, inexpensive, and constrained precision pointing-acquisition-tracking (PAT) systems. The transceivers incorporate MIMO-FSO terminals comprising M transmitters and N receivers, configured as illustrated in Figures 6 and 7. In this arrangement, $N-1$ receivers are distributed uniformly along the circumference of an imaginary circle of radius $\mathbb{R}_{\text{crl}}$ as shown in Figure 8, while a single receiver is positioned at the ring's center [64]. A corresponding configuration is employed for the M transmitters, which are oriented towards the center of the receiving ring. In the channel model (and in the simulations) only the receiver ring offset $\mathbb{R}_{\text{crl}}$ is used: the M transmit apertures are treated as co-located and each is aimed at the receiver, so the transmitter ring is only illustrative. The angle of arrival (AOA) is neglected of this communication link because of its negligible effect.The individual MIMO channels exhibit independent fading coefficients provided the separation between the transmitter and receiver units exceeds the channel's coherence length [65].

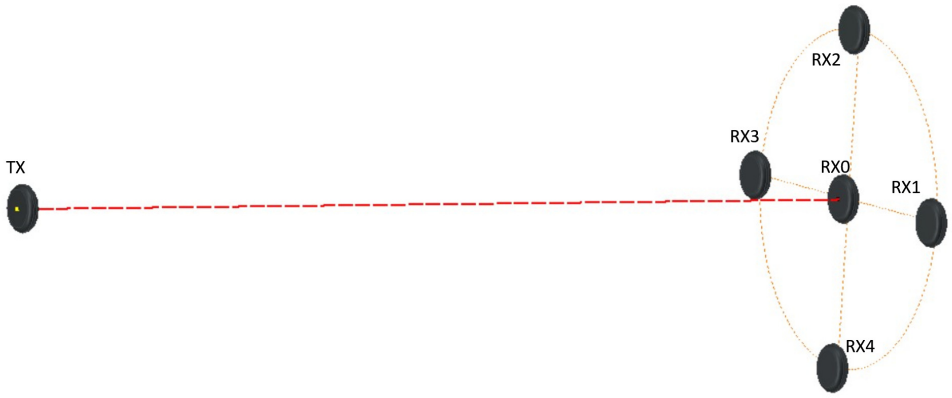


Fig. 6: SIMO aperture structure.

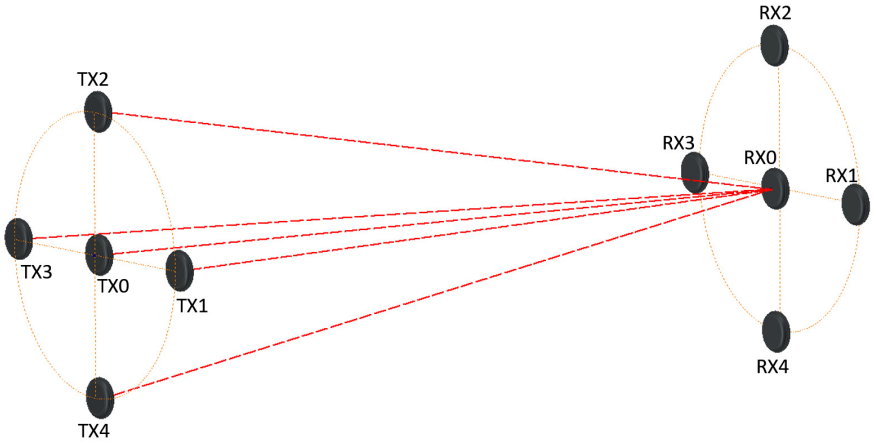


Fig. 7: MIMO aperture structure.

The ideal positions of transceivers' aperture are $(0, 0, Z_{u1})$ and $(0,\ Y_{u2},\ Z_{u2})$ with orientation $(\psi, 0)$ in Z-Y and Z-X plane, respectively. Because of random fluctuations in transceivers positions and orientations and considering the constrained precision of PAT system, the practical positions of transceivers' aperture will be $(\Delta x_1, \Delta y_1, Z_{u1} + \Delta z_1)$ and $(\Delta x_2, Y_{u2} + \Delta y_2, Z_{u2} + \Delta z_2)$. Here, Δx_1, Δy_1, Δz_1, Δx_2, Δy_2, and Δz_2 are zero-mean independent Gaussian random variables with variance σ_p^2. Moreover, the orientation of the UAV aperture deviates randomly from its nominal alignment $\psi, 0$ in the Z-Y and Z-X planes to a new state $\psi + \Delta\psi, \Delta\phi$. In this model, $\Delta\psi$ and $\Delta\phi$ represent independent Gaussian random variables with a zero mean and variance σ_ψ^2. Significant fluctuations in orientation induce random variations in the

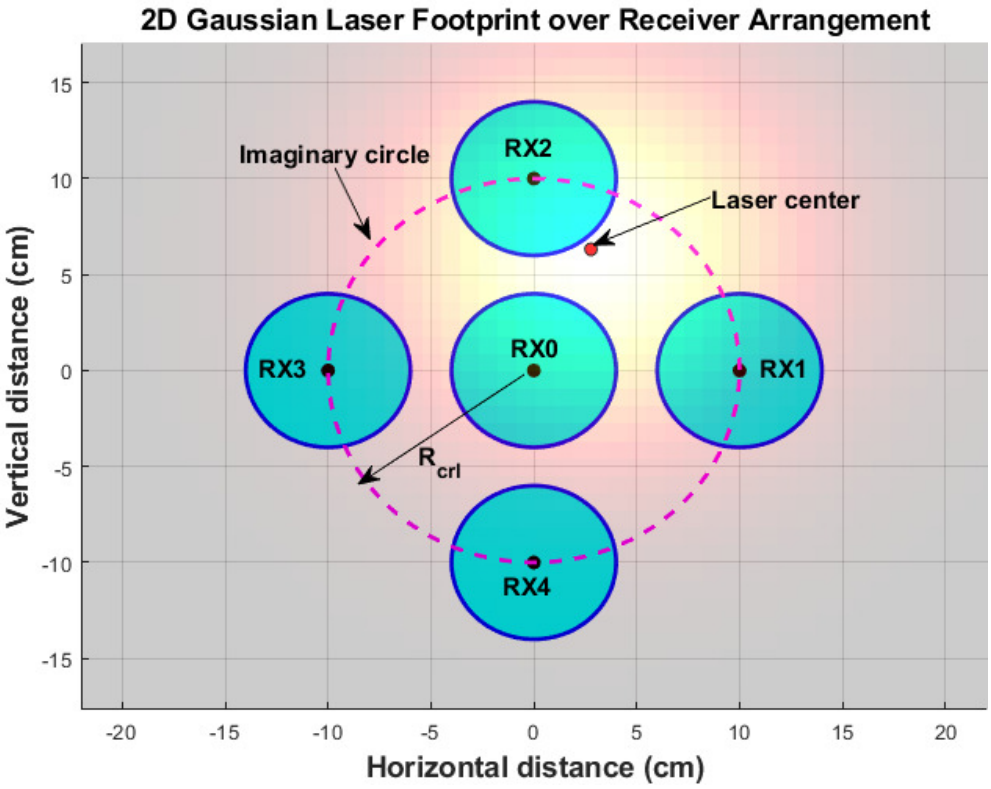


Fig. 8: MIMO aperture structure.

angles of arrival (AOAs) of the received beam and amplify radial displacements. The orientation errors enter the effective displacement variance as $\sigma_T^2 = 2\sigma_p^2 + \sigma_\psi^2 L^2$. With the PAT-corrected value $\sigma_\psi = 10^{-6}$ rad used here, $\sigma_\psi L \approx 1.2$ mm against $\sigma_p = 10$ cm, so the orientation term changes σ_T^2 by less than 10^{-4} in relative terms and the numerical results are governed by the position jitter alone; the orientation model would matter only if σ_ψ approached $\sigma_p/L \approx 85$ μrad. The resulting angle-of-arrival variations are negligible and are disregarded.

In the specified receiver configuration, photodetectors positioned on the imaginary circle experience non-zero boresight pointing errors characterized by a displacement of $\mathbb{R}_{\text{crl}}$. The combined effect of three-dimensional positional and orientational fluctuations in the transceivers is incorporated by projecting these deviations onto the aperture plane along the X and Y axes. Consequently, the aggregate radial displacement between the center of the received beam and the center of the j^{th} receiver is defined as $\Delta r_j = \sqrt{\Delta r_{xj}^2 + \Delta r_{yj}^2}$, where the components Δr_{xj} and Δr_{yj} follow the formulation of [66], re-derived here for ψ measured from the vertical. The line of sight is $\mathbf{u} = (0, \sin\psi, -\cos\psi)$, so the receiver aperture plane is spanned by $\mathbf{e}_x = (1, 0, 0)$

and $\mathbf{e}_y = (0, \cos\psi, \sin\psi)$. The beam centre in this plane is displaced by the transmitter shift, minus the receiver shift, plus the angular errors multiplied by L; projecting onto $\mathbf{e}_x$ and $\mathbf{e}_y$ gives

$$\begin{aligned}\Delta r_{xj} = &\left(\mathbb{R}_{\text{crl}} \cos\left(\theta_R^j\right) - L\,\Delta\phi\right) \\ &- (\Delta x_1 - \Delta x_2)\end{aligned} \tag{32}$$

$$\begin{aligned}\Delta r_{yj} = &\left(\mathbb{R}_{\text{crl}} \sin\left(\theta_R^j\right) - L\,\Delta\psi\right) \\ &- ((\Delta y_1 - \Delta y_2)\cos(\psi) + (\Delta z_1 - \Delta z_2)\sin(\psi))\,.\end{aligned} \tag{33}$$

Since the position errors are zero-mean, independent and symmetric, $\Delta x_1 - \Delta x_2$ and $\Delta x_1 + \Delta x_2$ (and likewise for y and z) have the same distribution, and because $\cos^2\psi + \sin^2\psi = 1$ the variance of each component is $2\sigma_p^2$ for any ψ. Here, θ_R^j is the angle of the j^{th} receiver location on circumference w.r.t. the X direction. Random displacements Δr_{xj} and Δr_{yj} are well described by Gaussian distribution with means $\mathbb{R}_{\text{crl}} \cos\left(\theta_R^j\right)$ and $\mathbb{R}_{\text{crl}} \sin\left(\theta_R^j\right)$, respectively, and variance $\sigma_T^2 = 2\sigma_p^2 + L^2\sigma_\psi^2$.

The receiver positioned at the ring's center experiences no boresight pointing error, as $\mathbb{R}_{\text{crl}} = 0$ and the total radial displacement over its aperture is described by Rayleigh distribution. Under the assumption of Gaussian beam shape, the pointing error loss seen by the j^{th} receiver is given by [33].

$$\begin{aligned}f_{h_p^j}\left(h_p^j\right) = &\frac{W_{\text{Leq}}^2}{4\sigma_T^2 A_o} \exp\left(-\frac{\mathbb{R}_{\text{crl}}^2}{2\sigma_T^2}\right)\left(\frac{h_p^j}{A_o}\right)^{\frac{W_{Leq}^2}{4\sigma_T^2}-1} \\ &I_o\left(\frac{\sqrt{-W_{\text{Leq}}^2\,\mathbb{R}_{\text{crl}}^2 \ln\left(\frac{h_p^j}{A_o}\right)}}{\sqrt{2}\sigma_T^2}\right)\end{aligned} \tag{34}$$

In this formulation, $I_o(\cdot)$ denotes the modified Bessel function of the first kind with zero order. The parameter A_o is defined as $(\text{erf}(v))^2$, where $v^2 = \frac{\pi a^2}{2W_L^2}$ and a represents the radius of the receiving aperture. The beam radius at the receiver plane is given by $W_L = \frac{D_T}{2} + L\,\theta_{div}$, where D_T is the transmitting-aperture diameter, $L = \frac{Z_{u1} - Z_{u2}}{\cos(\psi)}$ is the slant range, ψ is the angle between the link and the vertical, and θ_{div} is the optical beam-divergence angle in radians. Finally, the equivalent beam width is expressed as $W_{Leq}^2 = \frac{\sqrt{\pi} W_L^2 \text{erf}(v)}{2v\exp(-v^2)}$.

Beyond pointing inaccuracies, the FSO link is also affected by atmospheric turbulence. This impairment is commonly characterized using log-normal and Gamma-Gamma statistical distributions, which are applicable to weak and moderate-to-strong turbulence regimes, respectively. Proceeding with generality, we omit the indices in the subsequent analysis. The joint probability density function (PDF) for the composite

fading coefficient, defined as $h = h_p h_{at}$, is consequently provided by

$$f_h(h) = \int_0^\infty \frac{1}{h_{at}} f_{h_p}\left(h/h_{at}\right) f_{h_{at}}\left(h_{at}\right) dh_{at}. \tag{35}$$

Using (34) and making a variable change with $\zeta = \ln\left(\frac{A_o h_{at}}{h}\right)$ for simplification, we can rewrite (35) as

$$\begin{aligned} f_h(h) = &\int_0^\infty \frac{W_{Leq}^2}{4\sigma_T^2 A_o} \exp\left(-\varepsilon\left(\frac{W_{Leq}^2}{4\sigma_T^2} - 1\right)\right) \\ &\times \exp\left(-\frac{\mathbb{R}^2}{2\sigma_T^2}\right) I_o\left(\frac{\sqrt{W_{Leq}^2 \mathbb{R}^2 \varepsilon}}{\sqrt{2}\sigma_T^2}\right) f_{h_{at}}\left(\frac{h}{A_o}\exp(\varepsilon)\right) d\zeta. \end{aligned} \tag{36}$$

To solve (36), we apply generalized Gauss-Laguerre quadrature, i.e., $\int_0^\infty W(X) f(X) dX = \sum_{q=1}^{c} \Lambda_q f\left(v_q\right)$ [67] where $W(X)$ is defined $W(X) = (X-g)^{\alpha_2}\exp(-b(X-g))$, Λ_q and v_q are the Gauss-Laguerre weights and nodes respectively. In our case, we use $g = 0, \alpha_2 = 0$, and $b = \left(\frac{W_{Leq}^2}{4\sigma_T^2} - 1\right)$, which must be positive (i.e., $\delta^2 = W_{Leq}^2/(4\sigma_T^2) > 1$; here $\delta^2 \approx 71$ for the MIMO configuration). Therefore, (36) can be approximated as [68]

$$\begin{aligned} f_{h_{pa}}(h) \approx &\sum_{q=1}^{c} \frac{\Lambda_q W_{Leq}^2}{4\sigma_T^2 A_o} \exp\left(-\frac{\mathbb{R}^2}{2\sigma_T^2}\right) \\ &\times I_o\left(\frac{\sqrt{W_{Leq}^2 \mathbb{R}^2 v_q}}{\sqrt{2}\sigma_T^2}\right) f_{h_{at}}\left(\frac{h}{A_o}\exp\left(v_q\right)\right) \end{aligned} \tag{37}$$

with $\mathbb{R} = \mathbb{R}_{\text{crl}}$ for receivers at the ring circumference and $\mathbb{R} = 0$ for the receiver located at the center of the ring. This equation is general over the atmospheric turbulence effect, so it's equivalent to equations (17) with $\mathbb{R} = 0$. In addition, we will depend on equation (37) to build our MIMO model in the next section.

4.2 SNR Analysis with spatial diversity

Under maximum ratio combining (MRC) at the receiver side for the coherent system (MRC-C) shown in Figure (7), the instantaneous SNR at the combiner output is [40]

$$\gamma_{c,MRC} = \frac{C_c}{M} \sum_{m_t=1}^{M} \sum_{n_r=1}^{N} h_{pa,m_t n_r} \tag{38}$$

For SIM system using MRC (MRC-SIM), the instantaneous SNR at the combiner output is [40]

$$\gamma_{s,MRC} = \frac{C_s}{M} \sum_{m_t=1}^{M} \sum_{n_r=1}^{N} h_{pa,m_t n_r}^2 \tag{39}$$

For coherent system using EGC (EGC-C), the instantaneous SNR at the combiner output is [69]

$$\gamma_{c,EGC} = \frac{C_c}{MN} \left(\sum_{m_t=1}^{M} \sum_{n_r=1}^{N} \sqrt{h_{pa,m_t n_r}} \right)^2 \tag{40}$$

For SIM system using EGC (EGC-SIM), the instantaneous SNR at the combiner output is[40]

$$\gamma_{s,EGC} = \frac{C_s}{MN} \left(\sum_{m_t=1}^{M} \sum_{n_r=1}^{N} h_{pa,m_t n_r} \right)^2 \tag{41}$$

To find the SNR distributions for the four cases, it's necessary to find the distribution of $h_{\mathrm{M,m}}$ first

$$h_{\mathrm{M,m}} = \sum_{m_t=1}^{M} \sum_{n_r=1}^{N} h_{pa,m_t n_r}^{m} \tag{42}$$

where the mode of reception $m = 1, 2, 0.5,$ and 1 for MRC-C, MRC-SIM, EGC-C, and EGC-SIM respectively, and h_{M} is the sum of the MN link gains, each characterised by the PDF in (37). The atmospheric turbulence of different links is independent, but the pointing displacement is *common* to all apertures (Section 4.1) unlike [70] and [66]: the position and orientation jitter of the transceivers moves the whole beam, and only the deterministic ring offset differs between receivers. The terms of the sum are therefore not independent, and their moments are derived below by conditioning on the common displacement. The sum is well approximated by the $\alpha - \mu$ distribution, the PDF, CDF, and the moments of which are provided by [71].

$$f_{h_{\mathrm{M,m}}}(h_{\mathrm{M,m}}) \approx \frac{\alpha \mu^{\mu} h_{\mathrm{M,m}}^{\alpha\mu-1}}{\widehat{h}_{\mathrm{M,m}}^{\alpha\mu} \Gamma(\mu)} \exp\left(-\mu \frac{h_{\mathrm{M,m}}^{\alpha}}{\widehat{h}_{\mathrm{M,m}}^{\alpha}} \right) \tag{43}$$

$$F_{h_{\mathrm{M,m}}}(h_{\mathrm{M,m}}) \approx \bar{\mathbf{\Gamma}} \left(\mu \frac{h_{\mathrm{M,m}}^{\alpha}}{\widehat{h}_{\mathrm{M,m}}^{\alpha}}, \mu \right) \tag{44}$$

$$E\left[h_{\mathrm{M,m}}^{k}\right] \approx \frac{\widehat{h}_{\mathrm{M,m}}^{k} \Gamma(\mu + k/\alpha)}{\mu^{k/\alpha} \Gamma(\mu)} \tag{45}$$

where $\bar{\mathbf{\Gamma}}(s, x)$ is the regularized lower incomplete gamma function, the distribution parameters α and μ are positive real numbers , and $\widehat{h}_{\mathrm{MIMO}} = \sqrt[\alpha]{E\left[h_{\mathrm{MIMO}}^{\alpha}\right]}$ is an α-root mean value.

To calculate α, μ, and $\widehat{h}_{\mathrm{M}}$ for different m, we employ the moment-based parameter estimators [71], to solve the subsequent set of nonlinear equations:

$$\begin{aligned}
\frac{\Gamma^2(\mu+\frac{1}{\alpha})}{\Gamma(\mu)\Gamma(\mu+\frac{2}{\alpha})-\Gamma^2(\mu+\frac{1}{\alpha})} &= \frac{E^2\left[h_{\mathrm{M,m}}\right]}{E\left[h_{\mathrm{M,m}}^2\right]-E^2\left[h_{\mathrm{M,m}}\right]} \\
\frac{\Gamma^2(\mu+\frac{2}{\alpha})}{\Gamma(\mu)\Gamma(\mu+\frac{4}{\alpha})-\Gamma^2(\mu+\frac{2}{\alpha})} &= \frac{E^2\left[h_{\mathrm{M,m}}^2\right]}{E\left[h_{\mathrm{M,m}}^4\right]-E^2\left[h_{\mathrm{M,m}}^2\right]} \\
\widehat{h}_{\mathrm{M,m}} &= \frac{\mu^{\frac{1}{\alpha}}\Gamma(\mu)E\left[h_{\mathrm{M,m}}\right]}{\Gamma(\mu+\frac{1}{\alpha})}.
\end{aligned} \tag{46}$$

This nonlinear system can easily be solved by utilizing the fsolve built-in function that is included with MATLAB. By conditioning on the common pointing displacement $\mathbf{d}=(d_x,d_y)\sim\mathcal{N}(\mathbf{0},\sigma_T^2\mathbf{I}_2)$ (Section 4.1) and expanding the v^{th} power of the sum, the required moments $E\left[h_{\mathrm{M,m}}\right]$, $E\left[h_{\mathrm{M,m}}^2\right]$, and $E\left[h_{\mathrm{M,m}}^4\right]$ are

$$\begin{aligned}
E\left[h_{\mathrm{M,m}}^v\right] = \sum_{l_1=1}^{MN}\cdots\sum_{l_v=1}^{MN}\Big(\prod_{l=1}^{MN}E_{ATM}\left[h_{at}^{m\,n_l}\right]\Big) \\
\times\frac{A_o^{mv}}{1+2sv\sigma_T^2}\exp\Big(-s\sum_{i=1}^{v}\left|\boldsymbol{\varrho}_{l_i}\right|^2 \\
+\frac{s}{v}\Big|\sum_{i=1}^{v}\boldsymbol{\varrho}_{l_i}\Big|^2\frac{2sv\sigma_T^2}{1+2sv\sigma_T^2}\Big),
\end{aligned} \tag{47}$$

where $s=2m/W_{Leq}^2$, n_l is the number of indices l_i equal to l, and $\boldsymbol{\varrho}_l$ is the deterministic offset of the receiver of link l: $\boldsymbol{\varrho}_l=\mathbf{0}$ for the central receiver and $\boldsymbol{\varrho}_l=\mathbb{R}_{\mathrm{crl}}(\cos\theta_R^j,\sin\theta_R^j)$ for the j^{th} ring receiver, with $\theta_R^j=2\pi(j-1)/(N-1)$. The turbulence factor follows from the independence of the turbulence across links, and the pointing factor is the closed-form Gaussian integral $E_{\mathbf{d}}\big[\prod_i h_{p,l_i}^m\big]$ with $h_{p,l}=A_o\exp(-2|\boldsymbol{\varrho}_l-\mathbf{d}|^2/W_{Leq}^2)$, obtained by completing the square in $\mathbf{d}$. For $v=1$, (47) reduces to the sum of the individual link means, $E[h_{\mathrm{M,m}}]=\sum_l E_{ATM}[h_{at}^m]\,A_o^m\,(1+2s\sigma_T^2)^{-1}\exp\big(-s|\boldsymbol{\varrho}_l|^2/(1+2s\sigma_T^2)\big)$, which is the Rice-distribution moment used for a single link. For $v\geq 2$ it differs from the independent-link multinomial expansion of [71], which would be obtained by replacing the common displacement by independent ones; the two coincide when $\sigma_T\to 0$ and differ most when the jitter is large compared to the beam width.

The $\hat{K}^{\mathrm{th}}$ moments of the atmospheric turbulence are [72]:

$$E_{GG}\left[h_{at}^{\hat{K}}\right]=\left(\frac{1}{\rho_1\rho_2}\right)^{\hat{K}}\frac{\Gamma(\hat{K}+\rho_1)\Gamma(\hat{K}+\rho_2)}{\Gamma(\rho_1)\Gamma(\rho_2)} \tag{48}$$

$$E_{LN}\left[h_{at}^{\hat{K}}\right]=\exp\left(2\sigma_x^2\left(\hat{K}^2-\hat{K}\right)\right) \tag{49}$$

By substituting equations (48) and (47) into (46), we get α, μ, and $\widehat{h}_{\mathrm{MIMO}}$ for different m by solving the system of nonlinear equations. The moments in (47) were verified against Monte Carlo simulations with common jitter; for strong jitter ($\delta^2 \approx 9$–11) the independent-link expansion deviates from the simulated moments by up to 5% at $v = 4$, whereas (47) agrees within the Monte Carlo accuracy. For the parameters of Table 3 ($\delta \approx 8.4$) both give the same α-μ parameters to within 0.1%.

A visual assessment of Figures (9,10) reveals a strong correspondence between the analytical derivations and the simulation outcomes. For a more precise evaluation, Table (5) provides a quantitative measure by listing the mean squared error (MSE) between the derived α-μ CDF and the empirical CDF of 10^6 Monte Carlo samples with common pointing jitter, averaged over 200 histogram bins. This comparison is conducted across a broad spectrum of the refractive index structure parameter C_n^2, encompassing the most prevalent atmospheric turbulence models for both weak and strong regimes. The α-μ parameters are obtained by solving the moment equations to numerical convergence; for the log-normal case the solution lies on a nearly degenerate ridge (μ large, α small), so the LN fit is less accurate than the GG fit.

Table 5: MSE accuracy of CDF Derived Model.

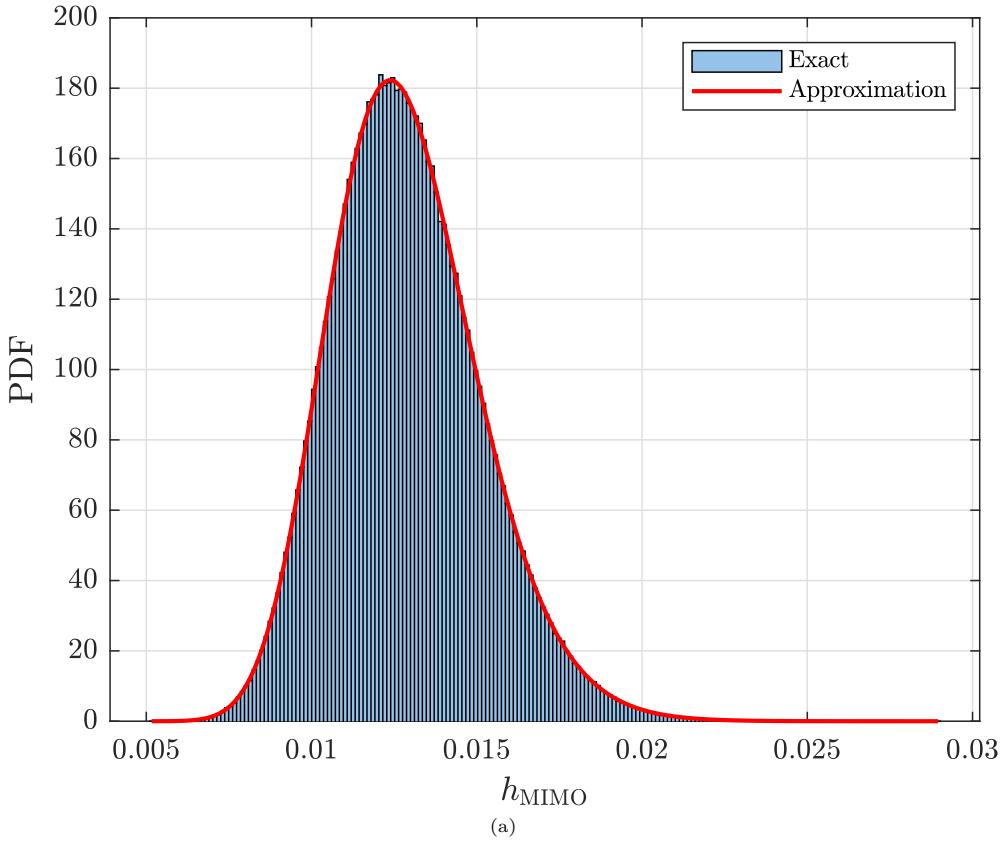
C_n^2	AT	SIMO(1,5)	MIMO(3,5)	MIMO(5,5)
5×10^{-15}	LN	2.18×10^{-6}	3.03×10^{-6}	2.85×10^{-6}
	GG	4.64×10^{-8}	1.62×10^{-7}	5.00×10^{-7}
2×10^{-14}	LN	6.71×10^{-6}	5.76×10^{-6}	4.64×10^{-6}
	GG	1.26×10^{-7}	1.84×10^{-8}	1.63×10^{-8}
1×10^{-13}	LN	1.04×10^{-5}	8.11×10^{-5}	7.03×10^{-5}
	GG	1.87×10^{-7}	9.81×10^{-8}	1.08×10^{-7}

Lower-tail accuracy.

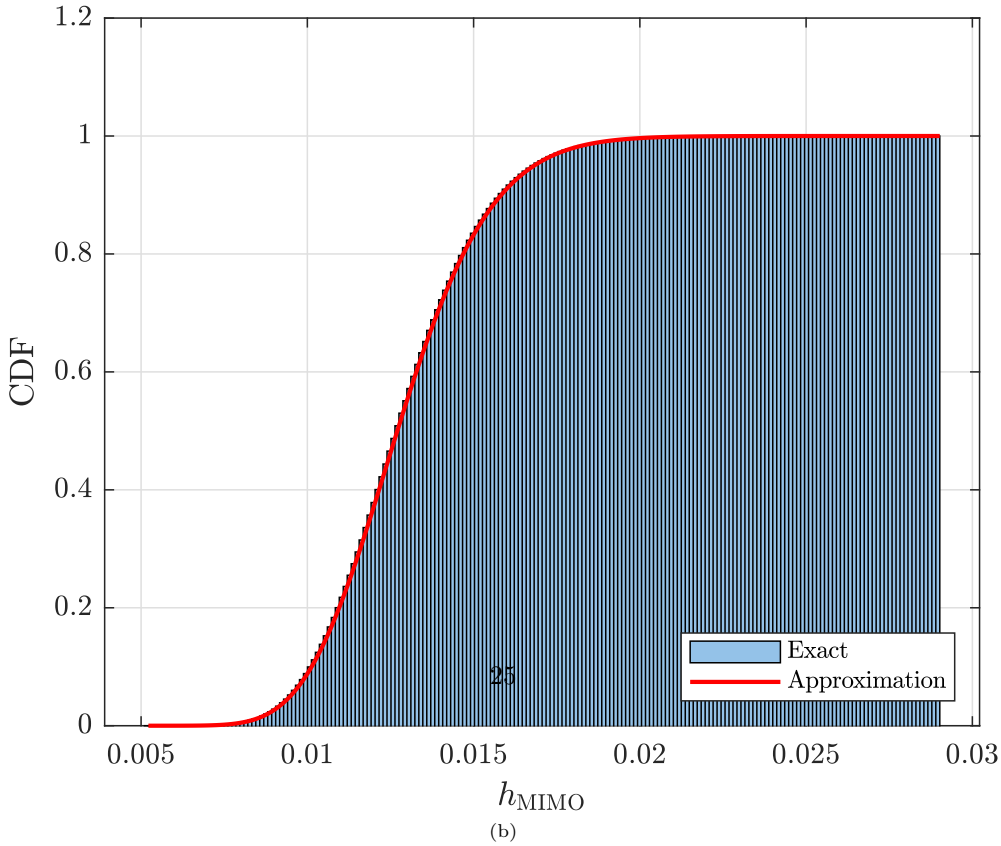
The linear-scale MSE in Table 5 cannot resolve the probabilities that matter for outage. Table 6 therefore compares, for $C_n^2 = 2\times10^{-14}$, the Monte Carlo probability $\mathrm{P}(h < h_p)$ with the nominal p, where h_p is the p-quantile of the fitted α-μ CDF (10^8 samples, accumulated in chunks of 10^7). For GG turbulence the fit is accurate to within 2–16% down to $p = 10^{-6}$ (≥ 100 events), so the analytic outage curves are reliable over the plotted range. For log-normal turbulence the moment-matched α-μ CDF overestimates the lower tail by a factor of about 2 at $p = 10^{-3}$ and by up to 10 at $p = 10^{-6}$ (conservative outage); the LN α-μ results should therefore be used only for the body of the distribution, not for deep-outage predictions.

Now, the instantaneous SNR can be obtained the by utilizing simple random variable transformation but the average SNR for coherent MRC at the combiner output is

$$\bar{\gamma}_{c,MRC} = \frac{C_c}{M} E\left[h_{\mathrm{M},1}\right] \tag{50}$$

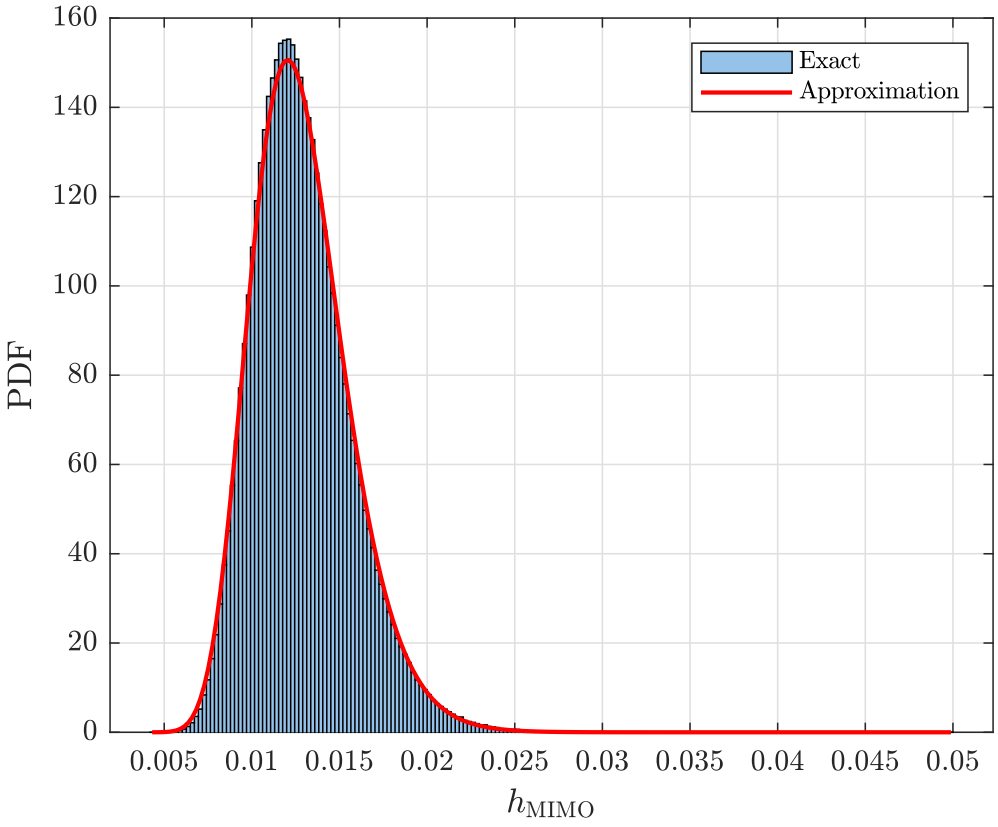


(a)

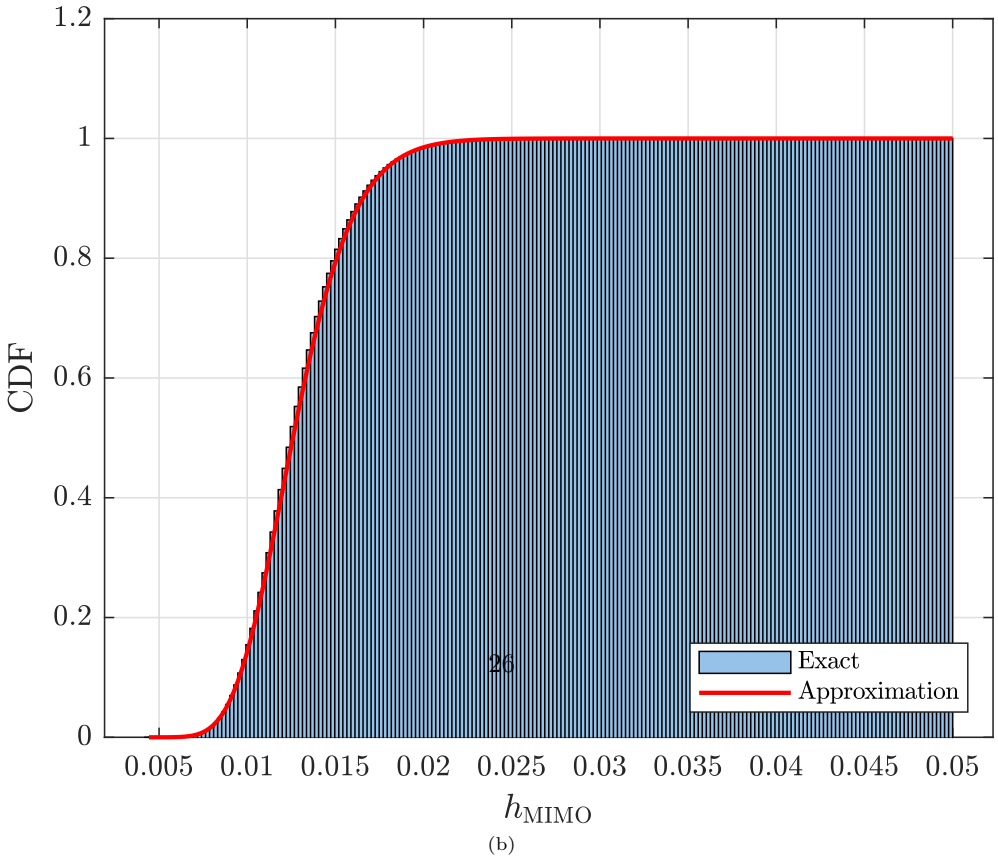


(b)

Fig. 9: MIMO(3,5) system with GG atmospheric turbulence with PE (a) PDF of h_{M}, (b) CDF of h_{M}.



(a)



(b)

Fig. 10: MIMO(3,5) system with LN atmospheric turbulence with PE (a) PDF of h_{M}, (b) CDF of h_{M}.

Table 6: Relative error $(\mathrm{P_{MC}} - p)/p$ of the fitted α-μ lower tail, 10^8 Monte Carlo samples. †fewer than 30 events.

	GG		LN	
p	MIMO(3,5)	SIMO(1,5)	MIMO(3,5)	SIMO(1,5)
10^{-3}	+2%	+5%	−49%	−51%
10^{-4}	+5%	+11%	−65%	−68%
10^{-5}	+7%	+16%	−80%	−78%
10^{-6}	+10%	+16%	−91%†	−83%

For SIM system using MRC, the average SNR at the combiner output is

$$\bar{\gamma}_{s,MRC} = \frac{C_s}{M} E\left[h_{\mathrm{M},2}\right] \tag{51}$$

For coherent system using EGC, the average SNR at the combiner output is

$$\bar{\gamma}_{c,EGC} = \frac{C_c}{MN} E\left[h^2_{\mathrm{M},0.5}\right] \tag{52}$$

For SIM system using EGC, the average SNR at the combiner output is

$$\bar{\gamma}_{s,EGC} = \frac{C_s}{MN} E\left[h^2_{\mathrm{M},1}\right] \tag{53}$$

So it is readily to consider $\bar{\gamma}_{\mathrm{comb}} = \frac{C_{system}}{MN_{comb}} E\left[h^{\varpi}_{\mathrm{M,m}}\right]$ where $C_{system} \in \{C_s, C_c\}$, $\varpi = 1$ or 2 for MRC and EGC respectively and $N_{comb} = 1$ or N for MRC and EGC respectively too. From equations (38), (39), (40), (41), it is easy to formulate a general instantaneous SNR expression as

$$\gamma_{\mathrm{M}} = \frac{\bar{\gamma}_{\mathrm{comb}}}{E\left[h^{\varpi}_{\mathrm{M,m}}\right]} h^{\varpi}_{\mathrm{M,m}} \tag{54}$$

where $E\left[h^{\varpi}_{\mathrm{M,m}}\right]$ is readily computed from equation (45).

By the analogy as in section (3.1) the relation between the channel state and the instantaneous SNR for the four cases is $h_{\mathrm{M,m}} = \sqrt[\varpi]{E\left[h^{\varpi}_{\mathrm{M,m}}\right] \gamma_{\mathrm{M}}/\bar{\gamma}_{\mathrm{comb}}}$. By utilizing this simple random variable transformation, depending on $h_{\mathrm{M,m}}$ distribution ($\alpha - \mu$ distribution) the resulting SNR PDF over the four cases is obtained by

$$\begin{aligned} f_{\gamma_{\mathrm{M}}}(\gamma_{\mathrm{M}}) \approx & \frac{\alpha}{\varpi \Gamma(\mu)} \vartheta_{\varpi}^{\mu} \gamma_{\mathrm{M}}^{\frac{\alpha\mu}{\varpi}-1} \\ & \exp\left(-\vartheta_{\varpi} \gamma_{\mathrm{M}}^{\frac{\alpha}{\varpi}}\right), \end{aligned} \tag{55}$$

where $\vartheta_{\varpi} = \left(\frac{\Gamma(\mu+\frac{\varpi}{\alpha})}{\Gamma(\mu)\bar{\gamma}_{\text{comb}}}\right)^{\frac{\alpha}{\varpi}}$. Then we have $\exp(-x)$ in terms of the Meijer-G function as $\exp(-x) = G_{0,1}^{1,0}\left[x\middle|_{0}^{-}\right]$ so, we can rewrite the previous equation as.

$$\begin{aligned} f_{\gamma_{\text{M}}}(\gamma_{\text{M}}) \approx & \frac{\alpha}{\varpi\Gamma(\mu)}\vartheta_{\varpi}^{\mu}\gamma_{\text{M}}^{\frac{\alpha\mu}{\varpi}-1} \\ & G_{0,1}^{1,0}\left[\vartheta_{\varpi}\gamma_{\text{M}}^{\frac{\alpha}{\varpi}}\middle|_{0}^{-}\right] \end{aligned} \tag{56}$$

this form will simplify the calculations of ASER and Ergodic Capacity. Then it is readily possible to calculate the moment generating function (MGF) of γ_{M} exactly, as an absolutely convergent integral over the underlying Gamma variable $U = \mu(h/\widehat{h})^{\alpha} \sim \text{Gamma}(\mu, 1)$ (for $t \leq 0$, which covers all error-rate evaluations, and for any ϖ/α). Expanding the exponential gives the power series $\sum_k \frac{t^k}{k!}\vartheta_{\varpi}^{-\varpi k/\alpha}\Gamma(\mu + \varpi k/\alpha)/\Gamma(\mu)$, which converges only for $\varpi/\alpha < 1$ and is therefore not used; the integral is evaluated by adaptive quadrature in the log domain and agrees with Monte Carlo averages,

$$M_{\gamma_{\text{M}}}(t) = \int_0^{\infty} \exp\left(t\,\vartheta_{\varpi}^{-\varpi/\alpha}u^{\varpi/\alpha}\right)\frac{u^{\mu-1}e^{-u}}{\Gamma(\mu)}\,du \tag{57}$$

4.3 Outage Probability

The outage probability expression of MIMO systems for the $\alpha-\mu$ distribution can be evaluated as

$$\begin{aligned} P_{\text{Out}}(\gamma_T) =& \text{Prob}\left(\gamma_{\text{M}} \leq \gamma_T\right) \\ =& \text{Prob}\left(\frac{\bar{\gamma}_{\text{comb}}}{E\left\{h_{\text{M,m}}^{\varpi}\right\}}h_{\text{M,m}}^{\varpi} \leq \gamma_T\right) \\ =& \text{Prob}\left(h_{\text{M,m}} \leq h_T\right) \\ =& F_{h_{\text{M,m}}}(h_T) \\ =& \bar{\mathbf{\Gamma}}\left(\mu\frac{h_T^{\alpha}}{\widehat{h}_{\text{M,m}}^{\alpha}}, \mu\right) \end{aligned} \tag{58}$$

where $h_T = \sqrt[\varpi]{E\left[h_{\text{M,m}}^{\varpi}\right]\gamma_T/\bar{\gamma}_{\text{comb}}}$ and $E\left[h_{\text{M,m}}^{\varpi}\right]$ is calculated from (45).

Consequently, this formulation possesses a general character, as the $\alpha-\mu$ distribution itself is a comprehensive fading model. It can be simplified to several other well-known distributions by adjusting its parameters; for instance, it becomes the Rayleigh distribution when $(\alpha = 2, \mu = 1)$, the Nakagami-m distribution when using μ as the fading parameter and $\alpha = 2$, and the Weibull distribution when α serves as the shape (fading) parameter and $\mu = 1$.

4.4 Ergodic Capacity

The normalized ergodic capacity corresponding to the considered MIMO FSO system in bits/s/Hz is defined as $C/B = \mathbb{E}\left[\log_2\left(1+\gamma_{\text{MIMO}}\right)\right]$, with $\mathbb{E}[\cdot]$ denoting expectation and B is the bandwidth. Hence, this ergodic capacity, C_{M}, can be obtained as follows

$$C/B = \underbrace{\int_0^{\infty}\cdots\int_0^{\infty}}_{\text{MN-fold}} \log_2\left(1+\sum_{i=1}^{MN}\gamma_i\right) f_{\gamma_1,\ldots,\gamma_{MN}}\left(\gamma_1,\ldots,\gamma_{MN}\right) d\gamma_1\cdots d\gamma_{MN}, \quad (59)$$

where γ_i is the i^{th} snr of the i^{th} link and the expectation is over their joint distribution. Since the combined SNR depends on the links only through $h_{\text{M,m}}$, whose α-μ approximation already accounts for the common pointing jitter, the expectation reduces, for both MRC ($\varpi = 1$) and EGC ($\varpi = 2$), to a single integral over the SNR of the combined channel,

$$C/B = \int_0^{\infty} \log_2\left(1+\gamma_{\text{M}}\right) pdf\left(\gamma_{\text{M}}\right) d\gamma_{\text{M}} \quad (60)$$

where $f_{\gamma_{\text{M}}}(\gamma_{\text{M}})$ is given by (56). To put the previous integral in standard form we use the rules $\log_n(x) = \ln(x)/\ln(n)$ and $\ln(1+x) = G_{2,2}^{1,2}\left[x \mid \begin{matrix}1,1\\1,0\end{matrix}\right]$ and then applying equation [07.34.21.0012.01] in [57], the MIMO unified expression for C/B is obtained as

$$C/B \approx A_{\varpi} H_{2,3}^{3,1}\left[\vartheta_{\varpi}\middle|\begin{matrix}(-\frac{\alpha\mu}{\varpi},\frac{\alpha}{\varpi}),(1-\frac{\alpha\mu}{\varpi},\frac{\alpha}{\varpi})\\(0,1),(-\frac{\alpha\mu}{\varpi},\frac{\alpha}{\varpi}),(-\frac{\alpha\mu}{\varpi},\frac{\alpha}{\varpi})\end{matrix}\right] \quad (61)$$

where $A_{\varpi} = \frac{\alpha}{\varpi\Gamma(\mu)\ln(2)}\left[\frac{\Gamma(\mu+\frac{\varpi}{\alpha})}{\Gamma(\mu)\bar{\gamma}_{\text{comb}}}\right]^{\frac{\alpha\mu}{\varpi}}$.

Because of complex calculations of H-fox function, we can re-derive the previous formula in the form of a Meijer-G function rather than a Fox-H function by using $\alpha = \frac{l}{z}$ to put the integral (60) in standard form [07.34.21.0011.01] in [57]. Then we have the following formula.

$$C/B \approx \boldsymbol{A}_{\varpi}^{G} G_{2l,z\varpi+2l}^{z\varpi+2l,l}\left[\boldsymbol{B}_{\varpi}^{G}\middle|\begin{matrix}Q_1\\Q_2\end{matrix}\right] \quad (62)$$

where the Meijer-G function amplitude is $\boldsymbol{A}_{\varpi}^{G} = \frac{A_{\varpi}\sqrt{z\varpi}}{l(2\pi)^{(l-1)+0.5(z\varpi-1)}}$, the Meijer-G function parameter is $\boldsymbol{B}_{\varpi}^{G} = \frac{B_{\varpi}^{z\varpi}}{(z\varpi)^{z\varpi}}$, and $Q_1 = \frac{-\frac{\alpha\mu}{\varpi}}{l},\ldots,\frac{l-1-\frac{\alpha\mu}{\varpi}}{l},\frac{1-\frac{\alpha\mu}{\varpi}}{l},\ldots,\frac{l-\frac{\alpha\mu}{\varpi}}{l}$, $Q_2 = 0,\ldots,\frac{z\varpi-1}{z\varpi},\frac{-\frac{\alpha\mu}{\varpi}}{l},\ldots,\frac{l-1-\frac{\alpha\mu}{\varpi}}{l},\frac{-\frac{\alpha\mu}{\varpi}}{l},\ldots,\frac{l-1-\frac{\alpha\mu}{\varpi}}{l}$ are the upper and lower Meijer-G function vectors respectively.

4.5 Average SER

ASER is obtained by integrating the conditional probability of symbol error $P_e(\gamma)$ with respect to the PDF of the received SNR.

$$ASER = \int_0^\infty P_e(\gamma) f_{\gamma_{FSO}}(\gamma) d\gamma \tag{63}$$

The chosen digital modulation strategy affects the expression of P_c. Here, we concentrate on the differential binary phase shift keying (DBPSK) where $ABER = C_{mod} M_{\gamma_M}(-D_{mod})$.

4.6 Numerical Results of MIMO-FSO Systems

To demonstrate the applicability of the preceding mathematical framework, this section presents numerical results for various performance indicators of a MIMO-FSO link transmission system. The FSO link is modeled as Gamma-Gamma fading channel with the effects of atmosphere for weak ($C_n^2 = 5 \times 10^{-15}$), moderate ($C_n^2 = 2 \times 10^{-14}$), and strong ($C_n^2 = 1 \times 10^{-13}$) turbulence FSO channels as in Table (3). The results of SISO system was obtained by using formulas derive in section (3) and they are going to be compared with MIMO-FSO results in this section.

For fair comparison, the photodetector radius in SISO system is square root of N times the photodetector radius in MIMO system resulting the same photodetecting area in both. In Figure (11), the Ergodic Capacity for coherent system is presented. The ergodic capacities of EGC and MRC are practically identical. To reach 5 bit/s/Hz, moving from SISO to MIMO(3,5) saves about 0.8 dB of average SNR for coherent detection, whereas in Figure (12) the saving for SIM is about 3.0 dB. In these comparison figures all schemes are normalized to the same average SNR, $\bar{\gamma} = \mathbb{E}[\gamma]$, so the SISO direct-detection curve differs slightly from the Ansari-normalized curves of the previous section. Because the FSO channel is slow fading, ergodic capacity is optimistic; Table 7 gives the capacity with outage for coherent detection (moderate turbulence). At an outage probability of $P_{\text{out}} = 10^{-3}$ the SISO rate falls 2.5–3.6 bit/s/Hz below its ergodic capacity, whereas MIMO(3,5) loses only 0.7–0.8 bit/s/Hz, so the benefit of diversity for a delay-constrained link is far larger than the ergodic comparison suggests.

Table 7: Ergodic capacity and capacity with outage $C_{\text{out}}(10^{-3})$ [bit/s/Hz], coherent detection, moderate turbulence ($C_n^2 = 2 \times 10^{-14}$), 4×10^6 Monte Carlo samples.

SNR	SISO		MIMO(3,5)		AWGN
[dB]	ergodic	C_{out}	ergodic	C_{out}	$\log_2(1+\bar{\gamma})$
10	3.22	0.75	3.44	2.73	3.46
20	6.36	2.96	6.64	5.84	6.66
30	9.66	6.11	9.95	9.13	9.97

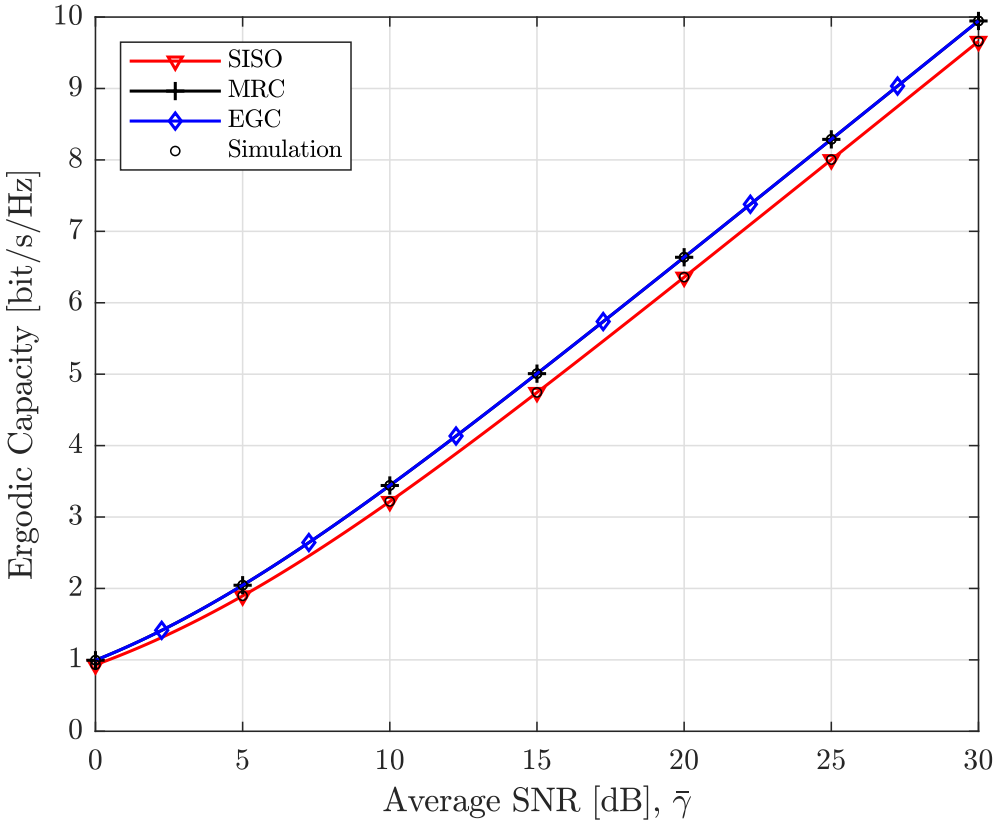


Fig. 11: Ergodic Capacity of coherent system in moderate turbulence with pointing error channel for SISO, and MIMO(3Tx,5Rx) arrangement versus Average SNR [dB].

In Figure (13), the outage probabilities of EGC and MRC verse SISO system is presented for coherent systems. At 10^{-5} outage probability, the combining methods outperform the SISO by about 13.6 dB; MRC and EGC are practically indistinguishable because the common pointing jitter correlates the links. On the other hand in Figure (14), the combiners outperform the SISO by about 28.0 (MRC) and 28.8 dB (EGC), and the EGC outperforms the MRC as the average SNR increases.

In Figure (15), the EGC performance seems as the MRC performance because the links are correlated through the common pointing jitter, which limits the diversity gain that distinguishes the two combiners. At 10^{-5} BER, the coherent systems are about 1.8–2.4 dB (EGC–MRC) better than the SIM systems and this gap reaches 3.3–4.1 dB at 10^{-10} BER. From these results, coherent detection is superior to SIM in both outage probability and ABER, at the cost of receiver complexity.

In Figure (16), the outage probabilities of SIMO-EGC and SIMO-MRC verse SISO system is presented for coherent and SIM systems. At 10^{-5} outage probability, SIMO(1,5) combining outperforms the SISO by about 10.8 dB for coherent detection and by 22.8 dB (both MRC and EGC) for SIM.

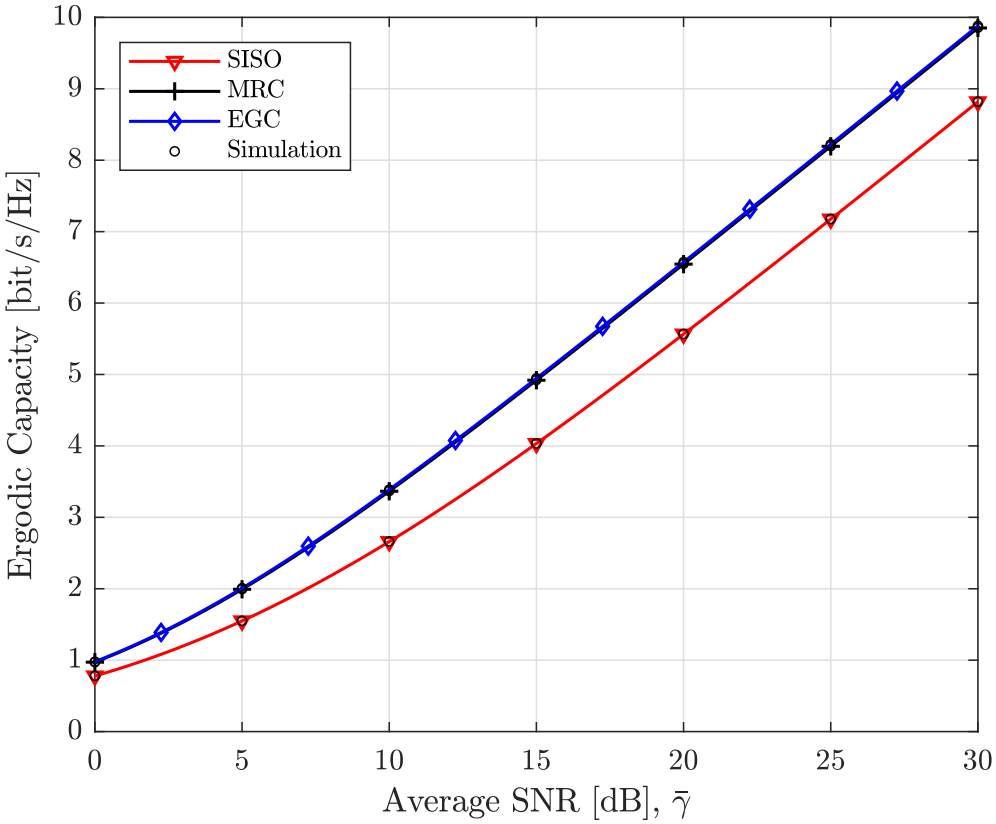


Fig. 12: Ergodic Capacity of SIM system in moderate turbulence with pointing error channel for SISO, and MIMO(3Tx,5Rx) arrangement versus Average SNR [dB].

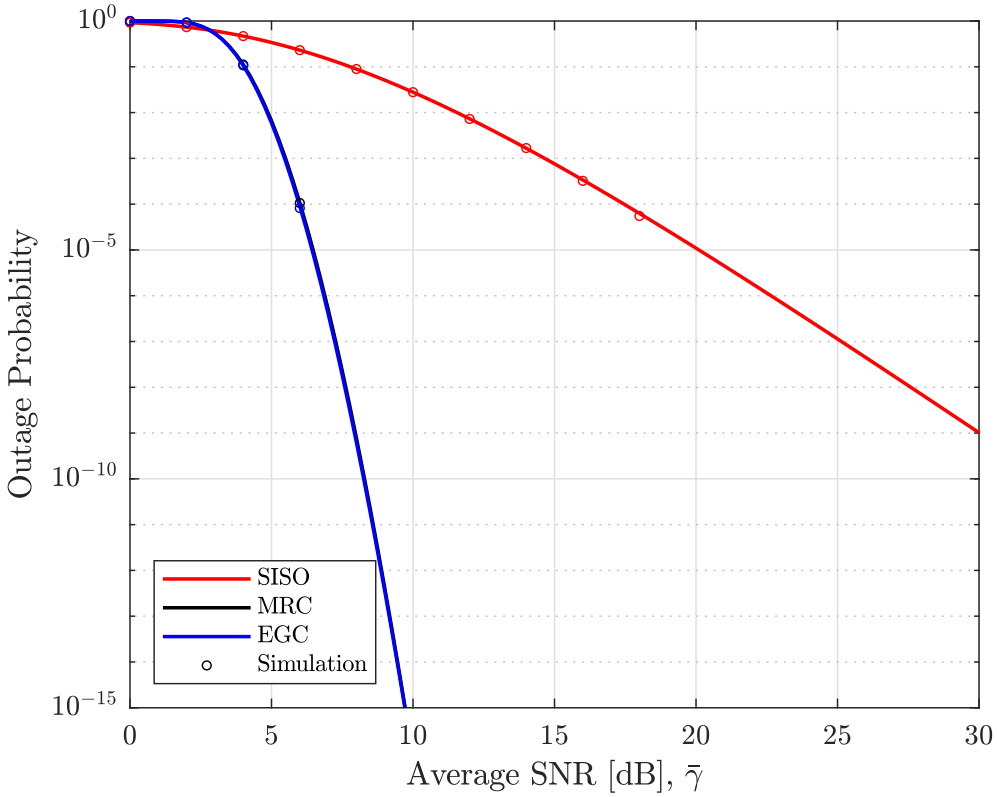


Fig. 13: Outage Probability of coherent systems in moderate turbulence with pointing error channel for SISO, and MIMO(3Tx, 5Rx) arrangement versus Average SNR [dB].

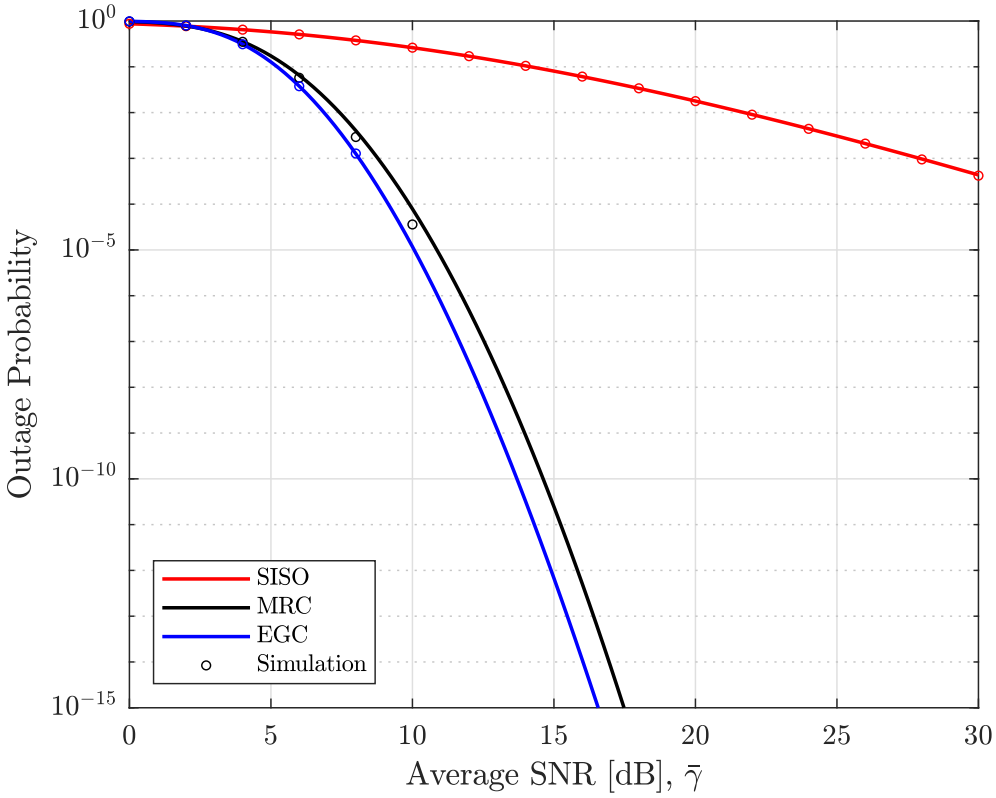


Fig. 14: Outage Probability of SIM systems in moderate turbulence with pointing error channel for SISO, and MIMO(3Tx, 5Rx) arrangement versus Average SNR [dB].

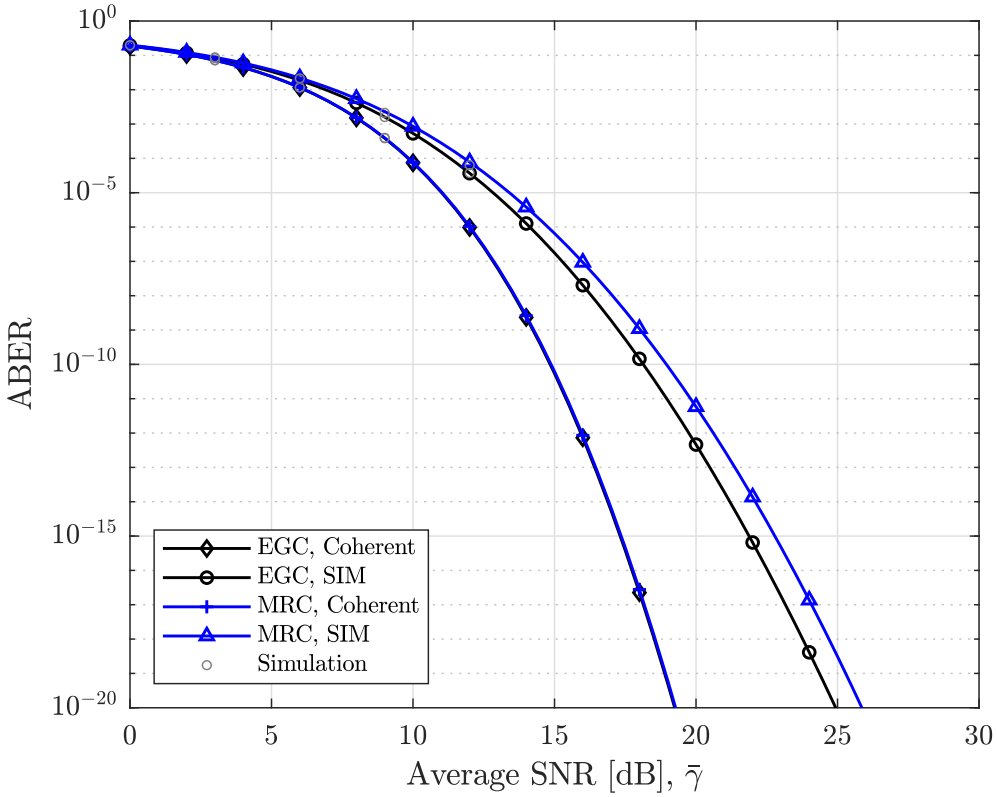


Fig. 15: ABER of MIMO(3Tx, 5Rx) systems in moderate turbulence with pointing error channel versus Average SNR [dB].

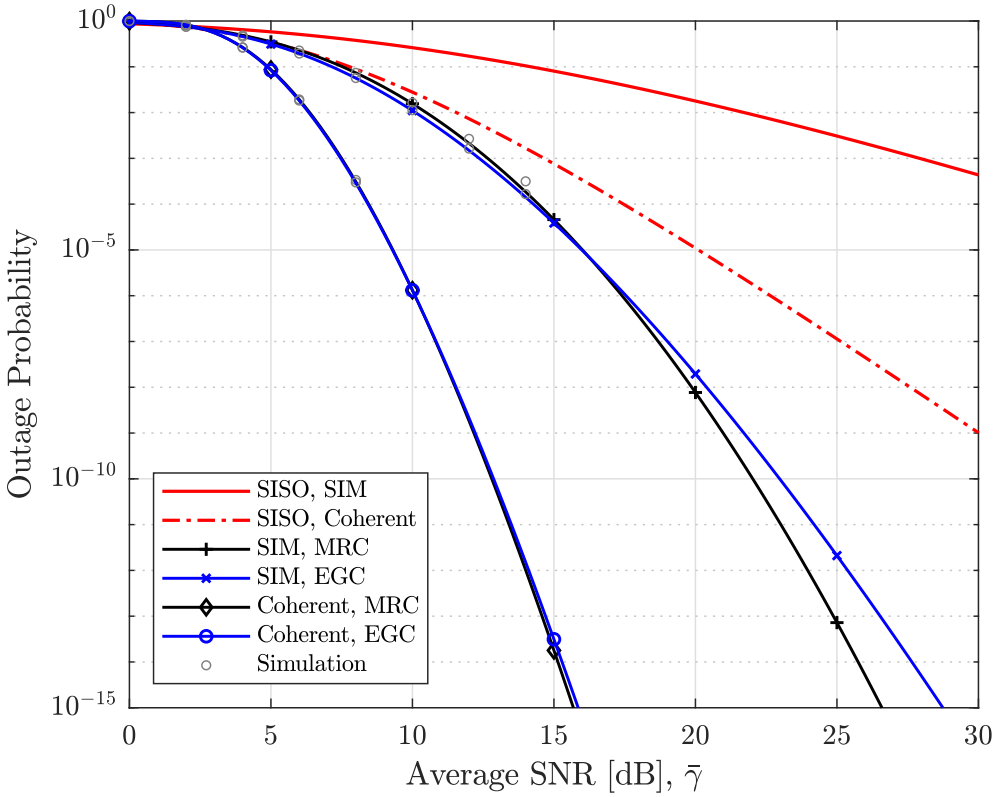


Fig. 16: Outage Probability of SIMO(1Tx, 5Rx) arrangement in moderate turbulence with pointing error channel for EGC, MRC, coherent, and SIM systems versus Average SNR [dB].

5 Conclusion and future work

In this work, the composite fading channel of atmospheric turbulence and pointing errors is presented, as well as a methodology of obtaining the performance of SISO-FSO horizontal and vertical links, including coherent and sub-carrier intensity modulation systems. Over and above, the performance of an equal gain combining and maximum ratio combining MIMO-FSO links are introduced over gamma-gamma and log-normal atmospheric turbulence with pointing errors, which can be extended to other turbulence models by changing the ν^{th} moment of the atmospheric turbulence coefficient in equation (47), provided the α-μ lower tail is validated (Table 6: accurate for GG, not for log-normal). Finally, this MIMO-FSO arrangement could be used to overcome the atmospheric turbulence effect, making links based on sub-carrier intensity modulation more reliable. In future work, the capacity with outage will be studied in addition to the study of various performance metrics under the assumption of transmitter and receiver CSI. Moreover, the spectral efficiency will be investigated.

Declarations

Competing interests

The authors declare no conflicts of interest.

Code availability

All MATLAB files used to generate the figures and tables (channel simulation, α-μ fitting, outage, capacity, ABER, tail validation and the GUI) will be made available in a public GitHub repository upon acceptance; until then they are available from the corresponding author on reasonable request.

Data availability

No external data were used. All simulated data are regenerated by the code with fixed random seeds.

References

[1] Roshdy, M.M., Elghandour, A.H., Hassan, K.M.: Free space optical communications: Challenges, mitigation techniques, classification framework, and standardization. Future Engineering Journal **5**(1) (2025)

[2] Alimi, I., Shahpari, A., Sousa, A., Ferreira, R., Monteiro, P., Teixeira, A., et al.: Challenges and opportunities of optical wireless communication technologies. Optical communication technology **10** (2017)

[3] Kawanishi, T.: Handbook of Radio and Optical Networks Convergence. Springer, Singapore (2024)

[4] Fernandes, M.A., Fernandes, G.M., Brandão, B.T., Freitas, M.M., Kaai, N., Der Wielen, B., Reid, J., Raiteri, D., Monteiro, P.P., Guiomar, F.P.: Unraveling "fiber in the sky": Terabit capacity enabled by coherent optical wireless. IEEE Communications Magazine **62**(3), 40–46 (2023)

[5] Alimi, I.A., Monteiro, P.P., Teixeira, A.L.: Analysis of multiuser mixed rf/fso relay networks for performance improvements in cloud computing-based radio access networks (cc-rans). Optics Communications **402**, 653–661 (2017)

[6] Khalighi, M.A., Uysal, M.: Survey on free space optical communication: A communication theory perspective. IEEE communications surveys & tutorials **16**(4), 2231–2258 (2014)

[7] Alimi, I., Shahpari, A., Ribeiro, V., Kumar, N., Monteiro, P., Teixeira, A.: Optical wireless communication for future broadband access networks. In: 2016 21st European Conference on Networks and Optical Communications (NOC), pp. 124–128 (2016). IEEE

[8] Kaymak, Y., Rojas-Cessa, R., Feng, J., Ansari, N., Zhou, M., Zhang, T.: A survey on acquisition, tracking, and pointing mechanisms for mobile free-space optical communications. IEEE communications surveys & tutorials **20**(2), 1104–1123 (2018)

[9] Musa, M.O., Naguib, M., Elghandour, A.H., Rohiem, A.E.: Channel modeling and pointing error mitigation in inter-satellite optical links using a dynamic beam waist adjustment method. AEU-International Journal of Electronics and Communications, 156246 (2026)

[10] Tsiftsis, T.A., Sandalidis, H.G., Karagiannidis, G.K., Uysal, M.: Optical wireless links with spatial diversity over strong atmospheric turbulence channels. IEEE Transactions on Wireless Communications **8**(2), 951–957 (2009)

[11] Zhu, X., Kahn, J.M.: Performance bounds for coded free-space optical communications through atmospheric turbulence channels. IEEE Transactions on communications **51**(8), 1233–1239 (2003)

[12] Uysal, M., Navidpour, S.M., Li, J.: Error rate performance of coded free-space optical links over strong turbulence channels. IEEE Communications Letters **8**(10), 635–637 (2004)

[13] Alimi, I.A., Shahpari, A., Monteiro, P.P., Teixeira, A.L.: Effects of diversity schemes and correlated channels on owc systems performance. Journal of Modern Optics **64**(21), 2298–2305 (2017)

[14] Zhu, X., Kahn, J.M.: Markov chain model in maximum-likelihood sequence detection for free-space optical communication through atmospheric turbulence channels. IEEE Transactions on Communications **51**(3), 509–516 (2003)

[15] Chan, V.W.: Free-space optical communications. Journal of Lightwave technology **24**(12), 4750–4762 (2006)

[16] Shin, E.J., Chan, V.W.: Optical communication over the turbulent atmospheric channel using spatial diversity. In: Global Telecommunications Conference, 2002. GLOBECOM'02. IEEE, vol. 3, pp. 2055–2060 (2002). IEEE

[17] Khalighi, M.-A., Schwartz, N., Aitamer, N., Bourennane, S.: Fading reduction by aperture averaging and spatial diversity in optical wireless systems. Journal of optical communications and networking **1**(6), 580–593 (2009)

[18] Lee, E.J., Chan, V.W.: Diversity coherent receivers for optical communication over the clear turbulent atmosphere. In: 2007 IEEE International Conference on Communications, pp. 2485–2492 (2007). IEEE

[19] Bayaki, E., Schober, R.: On space-time coding for free-space optical systems. IEEE Transactions on Communications **58**(1), 58–62 (2010)

[20] Bhatnagar, M.R., Anees, S.: On the performance of alamouti scheme in gamma-gamma fading fso links with pointing errors. IEEE Wireless Communications Letters **4**(1), 94–97 (2014)

[21] Jahid, A., Alsharif, M.H., Hall, T.J.: A contemporary survey on free space optical communication: Potentials, technical challenges, recent advances and research direction. Journal of network and computer applications **200**, 103311 (2022)

[22] Shakir, W.M., Mahdi, A.S., Hamdan, H., Charafeddine, J., Satai, H.A., Akrache, R., Haddad, S., Sayah, J.: Novel approximate distribution of the generalized turbulence channels for mimo fso communications. IEEE Photon. J **16**(4), 1–15 (2024)

[23] Anandkumar, D., Sangeetha, R.: Performance evaluation of ldpc-coded power series based malaga (m) distributed mimo/fso link with m-qam and pointing error. IEEE Access **10**, 62037–62055 (2022)

[24] Wilson, S.G., Brandt-Pearce, M., Cao, Q., Baedke, M.: Optical repetition mimo transmission with multipulse ppm. IEEE journal on Selected Areas in Communications **23**(9), 1901–1910 (2005)

[25] Fang, J., Bi, M., Xiao, S., Yang, G., Liu, L., Zhang, Y., Hu, W.: Polar-coded mimo fso communication system over gamma-gamma turbulence channel with spatially correlated fading. Journal of Optical Communications and Networking **10**(11), 915–923 (2018)

[26] Navidpour, S.M., Uysal, M., Kavehrad, M.: Ber performance of free-space optical transmission with spatial diversity. IEEE Transactions on wireless communications **6**(8), 2813–2819 (2007)

[27] Priyadarshani, R., Bhatnagar, M.R., Ghassemlooy, Z., Zvanovec, S.: Outage analysis of a simo fso system over an arbitrarily correlated m-distributed channel. IEEE Photonics Technology Letters **29**(24), 2191–2194 (2017)

[28] García-Zambrana, A., Castillo-Vázquez, C., Castillo-Vázquez, B., Hiniesta-Gómez, A.: Selection transmit diversity for fso links over strong atmospheric turbulence channels. IEEE Photonics Technology Letters **21**(14), 1017–1019 (2009)

[29] Garg, A., Bhatnagar, M.R., Berder, O., Vrigneau, B.: Imperfect-quantized-feedback-based beamforming for an fso miso system over gamma–gamma fading with pointing errors. Journal of optical communications and networking **9**(11), 1005–1018 (2017)

[30] Djordjevic, I.B., Vasic, B., Neifeld, M.A.: Multilevel coding in free-space optical mimo transmission with q-ary ppm over the atmospheric turbulence channel. IEEE photonics technology letters **18**(14), 1491–1493 (2006)

[31] Abou-Rjeily, C.: Performance analysis of fso communications with diversity methods: Add more relays or more apertures? IEEE Journal on Selected Areas in Communications **33**(9), 1890–1902 (2015)

[32] Qin, M., Chen, L., Wang, W.: Generalized selection multiuser scheduling for the mimo fso communication system and its performance analysis. IEEE Photonics Journal **8**(5), 1–9 (2016)

[33] Farid, A.A., Hranilovic, S.: Outage capacity optimization for free-space optical links with pointing errors. IEEE/OSA Journal of Lightwave Technology **25**(7), 1702–1710 (2007)

[34] BEA, S., Teich, M.: Fundamentals of photonics. Wiley, 313 (1991)

[35] Ricklin, J.C., Davidson, F.M.: Atmospheric turbulence effects on a partially coherent gaussian beam: implications for free-space laser communication. JOSA a **19**(9), 1794–1802 (2002)

[36] Farid, A.A., Hranilovic, S.: Outage capacity optimization for free-space optical links with pointing errors. Journal of Lightwave technology **25**(7), 1702–1710 (2007)

[37] Al-Habash, A., Andrews, L.C., Phillips, R.L.: Mathematical model for the irradiance probability density function of a laser beam propagating through turbulent media. Optical engineering **40**(8), 1554–1562 (2001)

[38] Roshdy, M., Hassan, K., Elghandour, A.: Unified performance parameters for im/dd techniques over gamma-gamma fading channel with pointing errors. In: Journal of Physics: Conference Series, vol. 2616, p. 012042 (2023). IOP Publishing

[39] Hasan, O.M.: Bit error rate and outage rate results for non-zero turbulence cells over gamma-gamma free-space optical wireless channel. J. Opt. commun. **34**(4), 385–391 (2013)

[40] Niu, M., Cheng, J., Holzman, J.F.: Error rate performance comparison of coherent and subcarrier intensity modulated optical wireless communications. Journal of Optical Communications and Networking **5**(6), 554–564 (2013)

[41] Gappmair, W.: Further results on the capacity of free-space optical channels in turbulent atmosphere. IET communications **5**(9), 1262–1267 (2011)

[42] Wang, N., Cheng, J.: Moment-based estimation for the shape parameters of the gamma-gamma atmospheric turbulence model. Optics express **18**(12), 12824–12831 (2010)

[43] Andrews, L.C., Phillips, R.L., Hopen, C.Y., Al-Habash, M.: Theory of optical scintillation. JOSA A **16**(6), 1417–1429 (1999)

[44] Andrews, L.C., Phillips, R.L.: Recent results on optical scintillation in the presence of beam wander. In: Atmospheric Propagation of Electromagnetic Waves II, vol. 6878, pp. 23–36 (2008). SPIE

[45] Andrews, L.C., Phillips, R.L., Sasiela, R.J., Parenti, R.: Pdf models for uplink to space in the presence of beam wander. In: Atmospheric Propagation IV, vol. 6551, pp. 92–103 (2007). SPIE

[46] Sandalidis, H.G., Tsiftsis, T.A., Karagiannidis, G.K.: Optical wireless communications with heterodyne detection over turbulence channels with pointing errors. Journal of lightwave technology **27**(20), 4440–4445 (2009)

[47] Elsaidy, E., Rakia, T.: A unified performance analysis of ogs-to-satellite fso uplink under turbulence and beam wander. In: 2022 5th International Conference on Communications, Signal Processing, and Their Applications (ICCSPA), pp. 1–6 (2022). IEEE

[48] Ansari, I.S., Alouini, M.-S., Yilmaz, F.: A unified performance analysis of free-space optical links over gamma-gamma turbulence channels with pointing errors (2013)

[49] Khallaf, H.S., Elfiqi, A.E., Shalaby, H.M., Sampei, S., Obayya, S.S.: On the performance evaluation of lqam-mppm techniques over exponentiated weibull fading free-space optical channels. Optics Communications **416**, 41–49 (2018)

[50] Yang, F., Cheng, J., Tsiftsis, T.A.: Free-space optical communication with nonzero boresight pointing errors. IEEE Transactions on Communications **62**(2), 713–725 (2014)

[51] Dabiri, M.T., Sadough, S.M.S., Khalighi, M.A.: Channel modeling and parameter optimization for hovering uav-based free-space optical links. IEEE Journal on Selected Areas in Communications **36**(9), 2104–2113 (2018)

[52] Jung, K.-J., Nam, S.S., Ko, Y.-C., Alouini, M.-S.: Ber performance of fso links over unified channel model for pointing error models. In: 2018 IEEE International Conference on Communications Workshops (ICC Workshops), pp. 1–6 (2018). IEEE

[53] Elsaidy, E., Rakia, T., Abdelaziz, M., Abd El-azeem, M.: Low-complexity joint transmit diversity and adaptive modulation schemes for ogs-satellite fso uplink. In: Journal of Physics: Conference Series, vol. 2616, p. 012043 (2023). IOP Publishing

[54] Youssef, A.A., Mohasseb, Y.Z.: Enhancing free space optical cubesat (fsocs) communication links using low-complexity ldpc decoding techniques. Scientific Reports **16**(1), 28196 (2026)

[55] Niu, M., Cheng, J., Holzman, J.F.: Error rate performance comparison of coherent and subcarrier intensity modulated optical wireless communications. IEEE/OSA Journal of Optical Communications and Networking **5**, 554–564 (2013)

[56] Goldsmith, A.: Wireless Communications. Cambridge University Press, Cambridge, UK (2005)

[57] http://functions.wolfram.com/constants/e/

[58] Navidpour, S.M., Uysal, M., Kavehrad, M.: Ber performance of free-space optical transmission with spatial diversity. IEEE Transactions on wireless communications **6**(8), 2813–2819 (2007)

[59] Kazemi, H., Uysal, M.: Performance analysis of mimo free-space optical communication systems with selection combining. In: 2013 21st Signal Processing and Communications Applications Conference (SIU), pp. 1–4 (2013). IEEE

[60] Cvijetic, N., Wilson, S.G., Brandt-Pearce, M.: Performance bounds for free-space optical mimo systems with apd receivers in atmospheric turbulence. IEEE Journal on Selected Areas in Communications **26**(3), 3–12 (2008)

[61] Bhatnagar, M.R., Ghassemlooy, Z.: Performance analysis of gamma–gamma fading fso mimo links with pointing errors. Journal of Lightwave technology **34**(9), 2158–2169 (2016)

[62] Dabiri, M.T., Saber, M.J., Sadough, S.M.S.: On the performance of multiplexing fso mimo links in log-normal fading with pointing errors. Journal of Optical Communications and Networking **9**(11), 974–983 (2017)

[63] Jaiswal, A., Abaza, M., Bhatnagar, M.R., Jain, V.K.: An investigation of performance and diversity property of optical space shift keying-based fso-mimo system. IEEE Transactions on Communications **66**(9), 4028–4042 (2018)

[64] Boluda-Ruiz, R., García-Zambrana, A., Castillo-Vázquez, B., Castillo-Vázquez, C.: Impact of nonzero boresight pointing error on ergodic capacity of mimo fso communication systems. Optics express **24**(4), 3513–3534 (2016)

[65] Chen, Z., Yu, S., Wang, T., Wu, G., Wang, S., Gu, W.: Channel correlation in aperture receiver diversity systems for free-space optical communication. Journal of Optics **14**(12), 125710 (2012)

[66] Khallaf, H.S., Uysal, M.: Uav-based fso communications for high speed train backhauling. In: 2019 IEEE Wireless Communications and Networking Conference (WCNC), pp. 1–6 (2019). IEEE

[67] Abramowitz, M., Stegun, I.A.: Handbook of Mathematical Functions with Formulas, Graphs, and Mathematical Tables. National Bureau of Standards,

Washington, DC (1964)

[68] Khallaf, H.S., Kato, K., Mohamed, E.M., Sait, S.M., Yanikomeroglu, H., Uysal, M.: Composite fading model for aerial mimo fso links in the presence of atmospheric turbulence and pointing errors. IEEE Wireless Communications Letters **10**(6), 1295–1299 (2021)

[69] Niu, M., Schlenker, J., Cheng, J., Holzman, J.F., Schober, R.: Coherent wireless optical communications with predetection and postdetection egc over gamma–gamma atmospheric turbulence channels. Journal of Optical Communications and Networking **3**(11), 860–869 (2011)

[70] Roshdy, M.M., El-Shazly, E.H., Mohamed, E.M., Elghandor, A., Hassan, K.M., Khallaf, H.S.: Performance analysis of uav-based mmw/fso relay-assisted system. In: 2023 International Telecommunications Conference (ITC-Egypt), pp. 429–434 (2023). IEEE

[71] Peppas, K.P.: A simple, accurate approximation to the sum of gamma–gamma variates and applications in mimo free-space optical systems. IEEE Photonics Technology Letters **23**(13), 839–841 (2011)

[72] Lim, H., Yoon, D.: Generalized moment-based estimation of gamma-gamma fading channel parameters. IEEE Transactions on Vehicular Technology **67**(1), 809–811 (2017)

Supplementary Files

This is a list of supplementary files associated with this preprint. Click to download.

- AllTablesmainnature.pdf